

RF DEPOLARIZING RESONANCES IN THE PRESENCE OF A FULL SIBERIAN SNAKE AND FULL SNAKE SPIN-FLIPPING

by

Boris B. Blinov

A dissertation submitted in partial fulfillment
of the requirements for the degree of
Doctor of Philosophy
(Physics)
in The University of Michigan
2000

Doctoral Committee:

Professor Alan D. Krisch, Chair
Professor Ratindranath Akhoury
Professor Ronald M. Gilgenbach
Associate Research Scientist Ali M.T. Lin
Professor Rudolf P. Thun

ABSTRACT

RF DEPOLARIZING RESONANCES IN THE PRESENCE OF A FULL SIBERIAN SNAKE AND FULL SNAKE SPIN-FLIPPING

by

Boris B. Blinov

Chairman: Alan D. Krisch

Frequent polarization reversals, or spin-flips, of a stored polarized beam in a high energy scattering asymmetry experiments may greatly reduce systematic errors of spin asymmetry measurements. A spin-flipping technique is being developed by using rf magnets running at a frequency close to the spin precession frequency, thereby creating spin-depolarizing resonances; the spin can then be flipped by ramping the rf magnet's frequency through the resonance. We studied, at the Indiana University Cyclotron Facility Cooler Ring, properties of such rf depolarizing resonances in the presence of a nearly-full Siberian snake and their possible application for spin-flipping. By using an rf-solenoid magnet, we reached a $98.7 \pm 1\%$ efficiency of spin-flipping. However, an rf-dipole magnet is more practical at high energies; hence, studies of spin-flipping by an rf-dipole are underway at IUCF.

For my wife

ACKNOWLEDGEMENTS

I would like to thank Professor Alan Krisch for his valuable advice, encouragement and support. I also thank my dissertation committee members their helpful comments and suggestions to this thesis. I thank my fellow collaborators from Michigan, Indiana, Protvino and Brookhaven for many hours they devoted to this experiment. I would especially like to thank Rick Phelps for teaching me a lot about how the experiment works.

I would like to thank the IUCF technical staff for their hard work on successful experiment operation. In particular, I want to thank the operators headed by Gary East with help from Terry Sloan for giving us beam when we needed it, the cryogenics experts Kevin Komisarcik and John Vanderwerp for keeping our snake cool, and the polarized ion source group headed by Vladimir Derenchuk for making polarized protons out of hydrogen gas.

Finally, I would like to thank my parents, my big brother and my little sister for their love and support, and my wife Svetlana for always being there when I needed her.

TABLE OF CONTENTS

DEDICATION	ii
ACKNOWLEDGEMENTS	iii
LIST OF TABLES	vi
LIST OF FIGURES	vii
 I. INTRODUCTION	 1
 II. THEORETICAL MOTIVATION	 5
II.1 Introduction	5
II.2 Spin Motion in a Magnetic Field	5
II.3 Spin Tune and Stable Spin Direction	9
II.4 RF Depolarizing Resonances	12
II.5 Froissart-Stora Formula and Spin-Flipping	16
 III. EXPERIMENTAL APPARATUS	 19
III.1 Introduction	19
III.2 Beam Acceleration in Cyclotrons and Polarization Rotation	20
III.3 Polarized Beam Injection into the Cooler Ring	21
III.4 The Cooler Ring	23
III.5 The Siberian Snake	24
III.6 The RF-Solenoid	27
III.7 The RF-Dipole	30
III.8 Polarimetry	32
 IV. EXPERIMENTAL RESULTS AND ANALYSIS	 35
IV.1 Introduction	35
IV.2 RF resonances	35
IV.2.1 Experimental procedure	36
IV.2.2 Data and Analysis	37
IV.3 RF depolarizing resonance widths	40

IV.4 Spin-flipping	43
IV.4.1 Experimental procedure	44
IV.4.2 Spin-flipping by varying the ramp time	44
IV.4.3 Spin-flipping by varying the frequency range	48
IV.4.4 Multiple spin-flipping	51
V. CONCLUSIONS	54
APPENDIX	56
BIBLIOGRAPHY	58

LIST OF TABLES

Table

III.1	McNaughton <i>et al.</i> [38] parameterization coefficients for A_n , which are valid between 100 and 450 MeV	34
IV.1	Typical electronics timing for rf depolarizing resonance study with a 30 second flattop.	37
IV.2	Locations and widths of rf depolarizing resonances at 104.1 MeV. . .	40
IV.3	Fit parameters for spin-flipping by varying the ramp time at 104.1 MeV.	46
IV.4	Summary of spin-flipping efficiencies	51

LIST OF FIGURES

Figure

II.1	A longitudinal rf magnetic field decomposition into two counter-rotating fields	13
II.2	Stable spin direction tilt in the rotating frame	14
II.3	Beam polarization after crossing an rf depolarizing resonance vs. ramp time	17
III.1	Indiana University Cyclotron Facility circa 1997-1998.	20
III.2	Injection hardware in the Cooler Ring	21
III.3	Beam positions in the Lambertson septum	22
III.4	The Cooler Ring	23
III.5	The Siberian snake	25
III.6	The Siberian snake solenoid layout	26
III.7	RF solenoid	28
III.8	RF solenoid's electronics	29
III.9	RF dipole (beam view)	31
III.10	RF dipole's electronics	31
III.11	Cooler polarimeter (top view).	33
IV.1	RF solenoid depolarizing resonances. The measured radial beam polarization at 104.1 MeV is plotted against the frequency of the rf solenoid.	38
IV.2	RF dipole depolarizing resonance. The measured radial beam polarization at 104.1 MeV is plotted against the frequency of the rf dipole.	39
IV.3	Possible rf dipole depolarizing resonance enhancement due to coherent betatron oscillations in a quadrupole.	42
IV.4	Spin-flipping while varying the rf solenoid's ramp time. The measured radial beam polarization at 104.1 MeV is plotted against the ramp time Δt . Arrows indicate the ramp times, used in spin-flipping while varying the frequency range, as described in Section IV.4.3.	45

IV.5	Spin-flipping while varying the rf dipole's ramp time. The measured radial beam polarization at 104.1 MeV is plotted against the ramp time Δt	47
IV.6	Spin-flipping by varying the rf solenoid's frequency range. The measured radial beam polarization at 104.1 MeV is plotted against the frequency range Δf	49
IV.7	Multiple spin-flipping using the rf solenoid. The measured radial beam polarization at 104.1 MeV is plotted against the number of spin-flips n	52

CHAPTER I

INTRODUCTION

Spin is one of the fundamental quantum numbers. Studying effects that involve spin is crucial for better understanding Nature. Such studies can be done using polarized beams, polarized targets, or both. While polarized proton targets are now widely used in a variety of experiments, when combined with a polarized proton beam they can provide much more information. Thus, developing a high-energy polarized proton beam for physics experiments is very useful; it is also very challenging.

In a circular accelerator, each proton's spin precesses around the vertical magnetic fields of the accelerator's ring's bending dipoles. At each point of the orbit, a vector called the **stable spin direction** (SSD) is defined such that the spin component along this direction remains unchanged from turn to turn. Any spin component, which is not aligned with the SSD, will precess around it, with a frequency called the **spin precession frequency** f_s that is related to the proton's circulation frequency f_c by:

$$f_s = f_c \nu_s, \tag{I.1}$$

where ν_s is the **spin tune**, which is the number of spin precessions during one turn around the ring.

If there are only vertical magnetic fields, then the polarization remains unchanged; however, any horizontal magnetic field can destroy the beam polarization. A **depo-**

larizing resonance occurs whenever there is a periodic horizontal magnetic field whose frequency is equal to the spin precession frequency; in terms of the tunes, this occurs when

$$\nu_s = n\nu_d + k, \quad (\text{I.2})$$

where ν_d is the tune of the depolarizing magnetic field, and n and k are integers. The spin tune ν_s is proportional to the proton's energy:

$$\nu_s = G\gamma, \quad (\text{I.3})$$

where $G=1.792847$ is the proton's anomalous magnetic moment, and γ is the Lorentz energy factor. Since a resonance occurs at least every 523 MeV, the protons will encounter many depolarizing resonances during acceleration to a high energy.

Three main types of depolarizing resonances exist in a circular accelerator ring. The first type, which is called an **imperfection resonance**, is caused by the imperfections in the ring's magnetic structure. An imperfection depolarizing resonance occurs whenever the spin tune is equal to an integer

$$\nu_s = n. \quad (\text{I.4})$$

The second type of depolarizing resonances is called an **intrinsic resonance**. These resonances are caused by the horizontal magnetic fields in the ring's quadrupoles, which are an intrinsic property of any strong focusing ring. The intrinsic depolarizing resonance condition is:

$$\nu_s = l\nu_x + m\nu_y + n, \quad (\text{I.5})$$

where ν_x and ν_y are the horizontal and vertical betatron tunes, while l , m and n are integers. The ν_y resonances are normally much stronger because the vertical oscillations move the protons into the horizontal fields of the quadrupoles.

The synchrotron oscillations of the protons' energy cause the third type of depolarizing resonance, which is called a **synchrotron depolarizing resonance**; its

resonance condition is:

$$\nu_s = k\nu_{sync} + n, \quad (\text{I.6})$$

where ν_{sync} is the synchrotron frequency, while k and n are integers.

Many experimental techniques have been proposed to overcome these depolarizing resonances. Some techniques involve complicated betatron tune manipulations to quickly “jump” through a resonance, or using special correction dipoles to overcome some other resonances [1, 2, 3, 4]. The main disadvantage of these methods is that each resonance must be corrected individually, which becomes impractical at very high energies, where there are many depolarizing resonances.

A more recent method, proposed by Derbenev and Kondratenko in 1978 [5], involves using a spin rotator called a **Siberian snake** that makes the spin tune equal to $1/2$ independent of the beam energy. This energy-independent ν_s eliminates most of the depolarizing resonances.

Once a polarized proton beam is accelerated to a high energy and stored, it is important to be able to reverse its polarization direction in order to reduce the systematic error in the asymmetry, measured in various polarized scattering experiments.

Studies at the IUCF Cooler Ring show that these polarization reversals (spin-flips) can be successfully done using an rf magnet. An rf magnet creates an **rf depolarizing resonance**, whose resonance condition is:

$$f_s = f_{rf} + nf_c, \quad (\text{I.7})$$

where f_{rf} is the frequency of the rf magnet, f_c is the protons’ circulation frequency, and n is an integer. By varying the rf magnet’s frequency from a value below the depolarizing resonance to a value above the resonance, one can **cross** the resonance. After such a crossing, the final beam polarization P_f is related to the initial beam polarization P_i via the **Froissart-Stora formula** [6]:

$$P_f = P_i \left[2e^{-\frac{(\pi \epsilon f_c)^2}{(\Delta f / \Delta t)}} - 1 \right], \quad (\text{I.8})$$

where ϵ is the resonance strength, and $\Delta f/\Delta t$ is the resonance crossing rate, while Δf is the frequency's range during its linear variation time Δt . The value of the exponent determines the final polarization. If the resonance strength is small and/or the crossing rate is fast, then the final polarization is very close to the initial polarization; this is called **fast crossing**. For larger resonance strengths and slower crossing rates, the exponent becomes larger, so that the exponential becomes smaller; then the final polarization can decrease towards zero; this is called **depolarization**. If the resonance is very strong and/or the crossing rate is very slow, then the value of the exponent is very large and the exponential approaches zero; therefore, the final polarization is reversed with respect to the initial polarization, while its absolute value is the same; this is called **spin flip**.

This thesis describes a spin-flipping experiment in the presence of a nearly-full Siberian snake at the IUCF Cooler Ring. Chapter II contains a brief discussion of polarized beam theory. I do not try to cover the whole field of polarized beam theory; instead I stress rf-induced depolarizing resonances and spin-flipping. Chapter III describes the experimental apparatus. In Chapter IV, the experimental results are discussed, while Chapter V contains the conclusions.

CHAPTER II

THEORETICAL MOTIVATION

II.1 Introduction

In this chapter we first discuss spin motion in the magnetic fields of a circular accelerator ring. The effects of a full and nearly full Siberian snake on the spin tune and the stable spin direction are then described. Later we discuss rf-induced resonances and their strength; we finish with discussions of the Froissart-Stora formula and spin-flipping by an rf-induced resonance .

II.2 Spin Motion in a Magnetic Field

The Thomas-BMT equation [7, 8] describes the behavior of a proton's spin polarization vector \vec{S} in a magnetic field \vec{B} and an electric field \vec{E} :

$$\frac{d\vec{S}}{dt} = \frac{e}{m_p\gamma} \vec{S} \times [(1 + G\gamma)\vec{B}_\perp + (1 + G)\vec{B}_\parallel - (G + \frac{1}{1+\gamma})\gamma\vec{\beta} \times \frac{\vec{E}}{c}], \quad (\text{II.9})$$

where m_p is the proton's rest mass and e is its charge, while \vec{B}_\perp and \vec{B}_\parallel are the magnetic field components transverse and parallel to the proton's velocity \vec{v} , and $\vec{\beta} = \vec{v}/c$. The electric and magnetic fields are measured in the laboratory frame, while the spin is defined in the proton's rest frame. The electric field term plays a

very minor role in the spin motion in a high energy circular accelerator; thus it can be neglected.

We shall use the curvilinear coordinate system, which rotates as one moves around the ring along a proton's ideal orbit; then the position is described as

$$\vec{r}(x, l, y) = \vec{r}_0(l) + x\hat{x} + y\hat{y}, \quad (\text{II.10})$$

where vector \vec{r}_0 defines a point on the ideal reference orbit which moves with an ideal proton, the unit vector \hat{x} points radially outward, and \hat{y} points vertically up. The third unit vector is defined as $\hat{l} = \frac{d\vec{r}_0}{dl}$, so that it points along the longitudinal velocity of the ideal proton.

Let us first consider the spin motion in the ring bending dipoles' vertical magnetic field:

$$\vec{B}_\perp = -B\hat{y}. \quad (\text{II.11})$$

Since \vec{B}_\parallel and \vec{E} are both negligible, Equation II.1 becomes:

$$\frac{d\vec{S}}{dt} = \frac{e}{m_p\gamma}\vec{S} \times [(1 + G\gamma)\vec{B}_\perp]. \quad (\text{II.12})$$

Inserting Equation II.11 we then obtain:

$$\frac{d\vec{S}}{dt} = \frac{eB}{m_p\gamma}(1 + G\gamma)(-S_l\hat{x} + S_x\hat{l}). \quad (\text{II.13})$$

Expanding and comparing the \hat{x} , \hat{l} and \hat{y} components, we get:

$$\frac{dS_x}{dt} = -\frac{eB}{m_p\gamma}(1 + G\gamma)S_l, \quad (\text{II.14})$$

$$\frac{dS_l}{dt} = \frac{eB}{m_p\gamma}(1 + G\gamma)S_x, \quad (\text{II.15})$$

$$\frac{dS_y}{dt} = 0. \quad (\text{II.16})$$

The solution for this system of differential equations is given by

$$S_x = S_h \cos\left(\frac{eB}{m_p\gamma}(1 + G\gamma)t\right), \quad (\text{II.17})$$

$$S_l = S_h \sin \left(\frac{eB}{m_p \gamma} (1 + G\gamma) t \right), \quad (\text{II.18})$$

$$S_y = S_v, \quad (\text{II.19})$$

where S_h is the horizontal component of the spin-polarization vector, and S_v is its vertical component; note that $S_h^2 + S_v^2 = 1$. Equations II.17-II.19 define the precession of the spin-polarization vector \vec{S} around the vertical axis with an angular velocity

$$\omega_v = \frac{eB}{m_p \gamma} (1 + G\gamma). \quad (\text{II.20})$$

Thus, when a proton passes through a dipole field of strength $\int B \cdot dl$, its spin-polarization rotates by an angle

$$\theta_S = \frac{e \int B \cdot dl (1 + G\gamma)}{\gamma m_p v}. \quad (\text{II.21})$$

Notice that, inside this dipole field, the proton's orbit bends by an angle

$$\theta_B = \frac{e \int B \cdot dl}{\gamma m_p v}; \quad (\text{II.22})$$

therefore, the spin precession angle in the proton's rest frame is:

$$\theta_{sp} = \frac{Ge \int B \cdot dl}{m_p v}. \quad (\text{II.23})$$

It can similarly be shown that a proton's spin would precess by this angle in any transverse magnetic field of strength $\int B \cdot dl$. Notice that this spin precession angle relates quite simply to the proton's bend angle, defined by Equation II.22, via

$$\theta_{sp} = G\gamma \theta_B. \quad (\text{II.24})$$

We can then relate the spin-polarization vector \vec{S}' after passing through a dipole to the initial spin vector \vec{S} by the matrix equation:

$$\vec{S}' = M(\theta) \vec{S}, \quad (\text{II.25})$$

where the dipole's precession matrix is given by:

$$M(\theta) = \begin{pmatrix} \cos(G\gamma\theta_B) & -\sin(G\gamma\theta_B) & 0 \\ \sin(G\gamma\theta_B) & \cos(G\gamma\theta_B) & 0 \\ 0 & 0 & 1 \end{pmatrix}. \quad (\text{II.26})$$

Now, consider a solenoidal field:

$$\vec{B}_{\parallel} = B\hat{l}. \quad (\text{II.27})$$

Since \vec{B}_{\perp} and \vec{E} are now negligible, the Equation II.1 simplifies to:

$$\frac{d\vec{S}}{dt} = \frac{e}{m_p\gamma}\vec{S} \times [(1+G)\vec{B}_{\parallel}]. \quad (\text{II.28})$$

Inserting Equation II.27, we obtain:

$$\frac{d\vec{S}}{dt} = \frac{eB}{m_p\gamma}(1+G)(-S_y\hat{x} + S_x\hat{y}). \quad (\text{II.29})$$

Again, expanding and comparing the \hat{x} , \hat{l} and \hat{y} components, we get:

$$\frac{dS_x}{dt} = -\frac{eB}{m_p\gamma}(1+G)S_y, \quad (\text{II.30})$$

$$\frac{dS_l}{dt} = 0, \quad (\text{II.31})$$

$$\frac{dS_y}{dt} = \frac{eB}{m_p\gamma}(1+G)S_x. \quad (\text{II.32})$$

Similarly, the solution is given by

$$S_x = S_{\perp} \cos\left(\frac{eB}{m_p\gamma}(1+G)t\right), \quad (\text{II.33})$$

$$S_l = \text{constant}, \quad (\text{II.34})$$

$$S_y = S_{\perp} \sin\left(\frac{eB}{m_p\gamma}(1+G)t\right), \quad (\text{II.35})$$

where $S_{\perp} = \sqrt{S_x^2 + S_y^2}$ is the transverse component of the spin-polarization vector \vec{S} and S_l is its longitudinal component; note that $S_{\perp}^2 + S_l^2 = 1$. As defined by

Equations II.33-II.35, the vector \vec{S} precesses around the longitudinal axis with an angular velocity

$$\omega_l = \frac{eB}{m_p\gamma}(1 + G). \quad (\text{II.36})$$

Using Equation II.36, one can show that when a proton with velocity \vec{v} passes through a solenoid field of strength $\int B \cdot dl$, its spin rotates by an angle

$$\theta_{sp} = \frac{(1 + G)e \int B \cdot dl}{\gamma m_p v} \quad (\text{II.37})$$

We shall define the **snake strength** s of a solenoid magnet as

$$s = \frac{\theta_{sp}}{\pi}. \quad (\text{II.38})$$

Combining Equation II.37 and Equation II.38, we can express the solenoidal field integral, required for a snake strength of s :

$$\int B \cdot dl = \frac{\pi s \gamma m_p v}{(1 + G)e} = 3.7521 \cdot s \cdot p, \quad (\text{II.39})$$

where p is the proton's momentum in GeV/c. Similarly to the dipole case, we can define the spin precession matrix inside a solenoid:

$$M(s) = \begin{pmatrix} \cos(\pi s) & 0 & -\sin(\pi s) \\ 0 & 1 & 0 \\ \sin(\pi s) & 0 & \cos(\pi s) \end{pmatrix}. \quad (\text{II.40})$$

II.3 Spin Tune and Stable Spin Direction

As shown in the previous section, the spin motion in a magnetic structure can be viewed as a precession around the magnetic field's direction. Thus, after one turn around a ring, the spin-polarization vector's direction at any point in the ring will usually differ from the vector's initial direction by some angle. This change in the spin-polarization vector's orientation can be described as a rotation around an axis,

called the **stable spin direction SSD**, by the single turn precession angle θ_{st} , which is proportional to the spin tune ν_s :

$$\theta_{st} = 2\pi\nu_s. \quad (\text{II.41})$$

In discussing the spin tune and the SSD, it is convenient to use the Pauli's spinor notation, where the spin is represented by a two-component complex spinor χ . The expectation value $\langle S_i \rangle$ of each component of the spin-polarization vector is:

$$\langle S_i \rangle = \chi^\dagger \sigma_i \chi, \quad (\text{II.42})$$

where the σ_i 's are the Pauli spin matrices. A rotation of the spin by an angle θ around an axis \hat{n} is then given by the transformation of the spinor χ into a spinor χ' , defined by:

$$\chi' = \exp\left(\frac{i\theta\vec{\sigma} \cdot \hat{n}}{2}\right) \chi \equiv M\chi, \quad (\text{II.43})$$

where M is the precession matrix. As a proton goes around a ring, it encounters many magnets, each with some spin precession matrix. Note that this matrix is a 2×2 matrix since it describes a transformation of the two-component spinor χ . The spinor χ after passing through n of these magnets will be transformed into a new spinor χ^n according to the equation:

$$\chi^n = M_n M_{n-1} \dots M_1 \chi, \quad (\text{II.44})$$

where M_i is the precession matrix in the i^{th} magnet; the product of these 2×2 matrices is also a 2×2 matrix.

After completing one turn around a ring, consisting of n magnets, a proton will have encountered all the magnetic fields once; the product of these n precession matrices is the ring's single-turn matrix M_{st} :

$$M_{st} = M_n M_{n-1} \dots M_1 = \exp\left(\frac{i2\pi\nu_s \vec{\sigma} \cdot \hat{n}^{SSD}}{2}\right), \quad (\text{II.45})$$

where \hat{n}^{SSD} is the unit vector of the stable spin direction (SSD), while $2\pi\nu_s$ is the angle of net spin rotation after one turn. It can be shown [9] that the spin tune is given by the trace of M_{st} :

$$\nu_s = \frac{1}{\pi} \cos^{-1} \left(\frac{\text{Tr}(M_{st})}{2} \right), \quad (\text{II.46})$$

and the components of the stable spin direction are given by:

$$n_i^{SSD} = \frac{1}{2i} \frac{\text{Tr}(\sigma_i M_{st})}{\sin(\pi\nu_s)}. \quad (\text{II.47})$$

Now we calculate the spin tune and the stable spin direction for two simple cases:

- a) an ideal ring with only the vertical magnetic fields of its bending dipoles,
- b) the same ideal ring with a full solenoidal snake installed.

In case *a*, with the dipole field pointing down, the spin rotates only around the vertical axis $-\hat{y}$; thus the SSD is vertical everywhere. The total spin precession angle is the sum of individual rotations around the vertical axis in each ring's dipole. Since the total bending angle in one turn is 2π , the single-turn spin precession angle is given by Equation II.24 to be:

$$\theta_{st} = 2\pi G\gamma. \quad (\text{II.48})$$

Comparing this to the Equation II.41, we find that for this ideal ring with only vertical field dipoles:

$$\nu_s = G\gamma. \quad (\text{II.49})$$

Now, to this ideal dipole ring we add a full Siberian snake solenoid magnet, having a snake strength $s = 1$. We consider a point on the ring orbit at an angle θ from the snake, which is at $\theta = 0$. The ring's single turn spin precession matrix is then the matrix product of: a dipole matrix with a vertical precession angle $G\gamma\theta$, a solenoid matrix with a longitudinal precession angle π , and another dipole matrix with a vertical precession angle $G\gamma(2\pi - \theta)$. Writing these matrices in the exponential form, we get:

$$M_{st}(\theta) = e^{-\frac{i}{2}\sigma_y G\gamma\theta} e^{-\frac{i}{2}\sigma_z \pi} e^{-\frac{i}{2}\sigma_y G\gamma(2\pi - \theta)}. \quad (\text{II.50})$$

Multiplying the exponentials and using the Pauli matrices relations, it can be shown [9] that:

$$\text{Tr}(M_{st}) = \cos(\pi G\gamma)\cos(\pi/2) = 0. \quad (\text{II.51})$$

Then from Equation II.46 the spin tune is given by:

$$\nu_s = \frac{1}{\pi}\cos^{-1}\left(\frac{1}{2}\text{Tr}(M_{st})\right) = 1/2; \quad (\text{II.52})$$

thus, ν_s is indeed independent of the proton's energy, as was mentioned in Chapter I. For an arbitrary snake strength s , one can show [9] that the spin tune is:

$$\nu_s = \frac{1}{\pi}\cos^{-1}\left(\cos(\pi G\gamma)\cos\left(\frac{\pi s}{2}\right)\right). \quad (\text{II.53})$$

Using Equations II.47 and II.50, we can also obtain the normalized components of the SSD:

$$n_x = \sin(G\gamma(\theta - \pi)), \quad (\text{II.54})$$

$$n_l = -\cos(G\gamma(\theta - \pi)), \quad (\text{II.55})$$

$$n_y = 0. \quad (\text{II.56})$$

Thus, the stable spin direction is always **horizontal** when one full Siberian snake is present, while the radial and the longitudinal components change as the SSD rotates by an angle $G\gamma$ during each turn around the ring.

II.4 RF Depolarizing Resonances

An rf magnetic field from either an rf solenoid or an rf dipole magnet can depolarize the beam. This depolarization occurs when the frequency of the rf magnet satisfies the resonance condition, given by Equation I.7.

Consider a proton stored in an accelerator ring. Assume that its spin tune is far away from any imperfection or intrinsic resonance condition; the spin of the proton then precesses unperturbed around the vertical fields of the bending dipoles at a

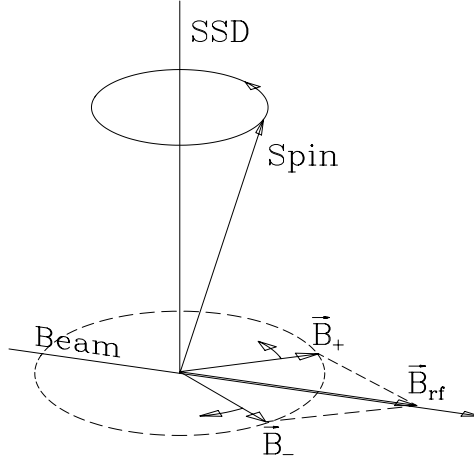


Figure II.1: A longitudinal rf magnetic field decomposition into two counter-rotating fields frequency ω_s , as measured in the laboratory frame. Now introduce an rf field of amplitude B , direction \hat{i} and frequency ω_{rf} :

$$\vec{B}_{rf} = B \cos(\omega_{rf} t) \hat{i}. \quad (\text{II.57})$$

Now assume that $\hat{i} = \hat{l}$, so that the rf field is longitudinal; the following discussion can also be applied to the case of a transverse field. This longitudinal rf magnetic field can be decomposed into two constant-magnitude counter-rotating fields \vec{B}_+ and \vec{B}_- of amplitude $\frac{1}{2}B$ and frequency ω_{rf} :

$$\vec{B}_+ = \frac{B}{2} (\cos(\omega_{rf} t) \hat{l} + \sin(\omega_{rf} t) \hat{x}), \quad (\text{II.58})$$

$$\vec{B}_- = \frac{B}{2} (\cos(\omega_{rf} t) \hat{l} - \sin(\omega_{rf} t) \hat{x}). \quad (\text{II.59})$$

The field \vec{B}_+ rotates in the same direction as the spin vector; the field \vec{B}_- rotates in the opposite direction, as shown in Figure II.1. If the frequency ω_{rf} is far away from the spin precession frequency ω_s , the total effect of these fields on the spin averages to zero. However, if ω_{rf} is close to ω_s , the rotation of the spin vector becomes correlated with the rotation of \vec{B}_+ , which can tilt the stable spin direction. To quantify this tilt, consider the frame that rotates around the stable spin direction

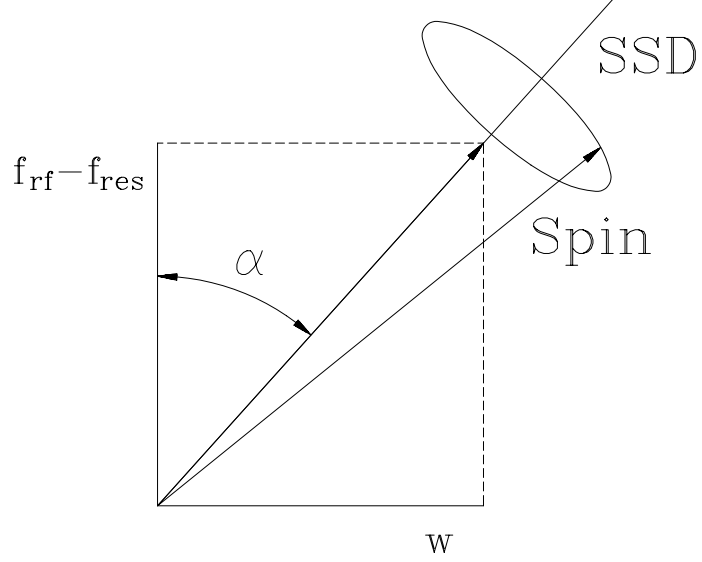


Figure II.2: Stable spin direction tilt in the rotating frame

with the spin precession frequency ω_s . As shown in Figure II.2, in this frame the stable spin direction would be tilted from vertical by the angle α given by:

$$\cos(\alpha) = \frac{f_{rf} - f_{res}}{\sqrt{(f_{rf} - f_{res})^2 + (\epsilon f_c)^2}}, \quad (\text{II.60})$$

where $f_{rf} = \frac{\omega_{rf}}{2\pi}$ is the rf magnet's frequency, f_{res} is the resonance's central frequency, f_c is the circulation frequency, and ϵ is the resonance's strength, which is proportional to the integrated rf magnetic field's amplitude $\int B_{rf} \cdot dl$:

$$\epsilon = \frac{(1 + G)e}{\gamma m_p v} \frac{\int B_{rf} \cdot dl}{2}. \quad (\text{II.61})$$

Note that only one half of the rf magnetic field amplitude contributes, because only one of the two counter-rotating fields induces the resonance.

In the laboratory frame, this tilt would result in an apparent depolarization, since the horizontal component of the polarization would average to zero. If an rf magnet was turned on abruptly at frequency f_{rf} , the vertical beam polarization with an initial value P_0 would be reduced to:

$$P = P_0 [\cos(\alpha)]^2 = P_0 \frac{(f_{rf} - f_{res})^2}{(f_{rf} - f_{res})^2 + (\epsilon f_c)^2}, \quad (\text{II.62})$$

which is a first-order Lorentzian in the rf frequency.

However, it has been observed [10] that the actual measured width w of an rf depolarizing resonance is not always equal to its normalized strength ϵf_c , as theory predicts; in fact, the measured width is frequently wider than the normalized resonance strength. Moreover, the shape of the resonance curve does not always follow a first-order Lorentzian. Several mechanisms for this resonance width enhancement have been proposed, including: a large beam energy spread, which could increase the resonance width for either an rf solenoid or an rf dipole; and large coherent betatron oscillations, caused by an rf dipole. They will be discussed in Chapter IV.

The frequency f_{res} at which an rf depolarizing resonance is centered can be predicted from Equation I.7 by knowing the circulation frequency f_c and the spin tune ν_s . Here we are mainly interested in the rf depolarizing resonances in the presence of a full or a nearly full Siberian snake.

First, consider a nearly full Siberian snake, whose snake strength s is very close but not exactly equal to 1. Let us assume that the snake strength is less than 1 by a very small amount δs . Then the spin tune, defined by Equation II.53, is:

$$\nu_s = \frac{1}{\pi} \cos^{-1} \left\{ \cos(\pi G \gamma) \cos\left(\frac{\pi(1 - \delta s)}{2}\right) \right\}. \quad (\text{II.63})$$

For very small δs this simplifies to:

$$\nu_s \simeq 1/2 - \frac{\delta s}{2} \cos(\pi G \gamma). \quad (\text{II.64})$$

According to Equation I.7, rf depolarizing resonances will occur at the frequencies:

$$f_{rf} = f_c \left\{ n \pm \left[1/2 - \frac{\delta s}{2} \cos(\pi G \gamma) \right] \right\}, \quad (\text{II.65})$$

where n is an integer. Thus, for each n , there will be two resonances, which are closely spaced around $f_c(n + 1/2)$ at frequencies:

$$f_l = f_c \left[n + \left(1/2 - \frac{\delta s}{2} \cos(\pi G \gamma) \right) \right] = f_c \left[n + 1/2 - \frac{\delta s}{2} \cos(\pi G \gamma) \right] \quad (\text{II.66})$$

and

$$f_u = f_c[(n+1) - (1/2 - \frac{\delta s}{2} \cos(\pi G \gamma))] = f_c[n + 1/2 + \frac{\delta s}{2} \cos(\pi G \gamma)]; \quad (\text{II.67})$$

the subscript l refers to a **lower**-frequency resonance, and subscript u refers to an **upper**-frequency resonance. These resonances are separated by

$$\delta f = f_u - f_l = f_c \delta s \cos(\pi G \gamma). \quad (\text{II.68})$$

If this separation δf is comparable to the resonances' widths, then the two resonances may overlap.

Now, consider the rf depolarizing resonances frequencies in the presence of an exactly 100% Siberian snake. From Equation II.48, the spin tune is then equal to exactly 1/2, and expression for the lower and the upper resonance frequencies from Equations II.66 and II.67 coincide:

$$f_l = f_u = f_c(n + 1/2), \quad (\text{II.69})$$

where n is an integer. Thus, with an exactly 100% snake, there would be a pair of completely overlapping rf depolarizing resonances, located at each half-integer value of the circulation frequency.

II.5 Froissart-Stora Formula and Spin-Flipping

Now consider a proton beam, stored in an accelerator ring with an rf magnet, whose frequency f_{rf} is very far from the resonance frequency f_{res} ; for example, let $f_{rf} = f_{res} - \Delta f/2$. The tilt angle α is then very small and the polarization is nearly perfectly vertical. Now let the rf magnet's frequency increase monotonously by some amount Δf in some time Δt , so that at some instant $f_{rf} = f_{res}$, and then later $f_{rf} = f_{res} + \Delta f/2$. According to Equation II.60, the SSD, will then tilt from the vertical and will cross the horizontal plane when $f_{rf} = f_{res}$; it will reverse to the

opposite direction at the end of the frequency ramp at time Δt . If the frequency ramp rate $\Delta f/\Delta t$ is sufficiently slow, then the spin would follow the SSD, and flip.

Froissart and Stora [6] derived an equation to relate the final beam polarization, P_f , to the initial polarization P_i , which was given earlier as Equation I.5:

$$P_f = P_i [2e^{-\frac{(\pi\epsilon f_c)^2}{(\Delta f/\Delta t)}} - 1]; \quad (\text{II.70})$$

note that ϵ is the resonance strength and $\Delta f/\Delta t$ is the frequency variation rate, where Δf is the frequency range during the frequency ramp time Δt (assuming a constant rate). As discussed the Chapter I, depending on the values of $\Delta f/\Delta t$ and the resonance strength, such a ramp could cause either partial or full depolarization or partial or full spin-flip. The final polarization P_f is plotted against Δt , assuming $P_i = 1$, in Figure II.3.

However, the Froissart-Stora formula is only exactly valid for an isolated resonance, and for a frequency range varying from $-\infty$ to $+\infty$. In practice, depolarizing

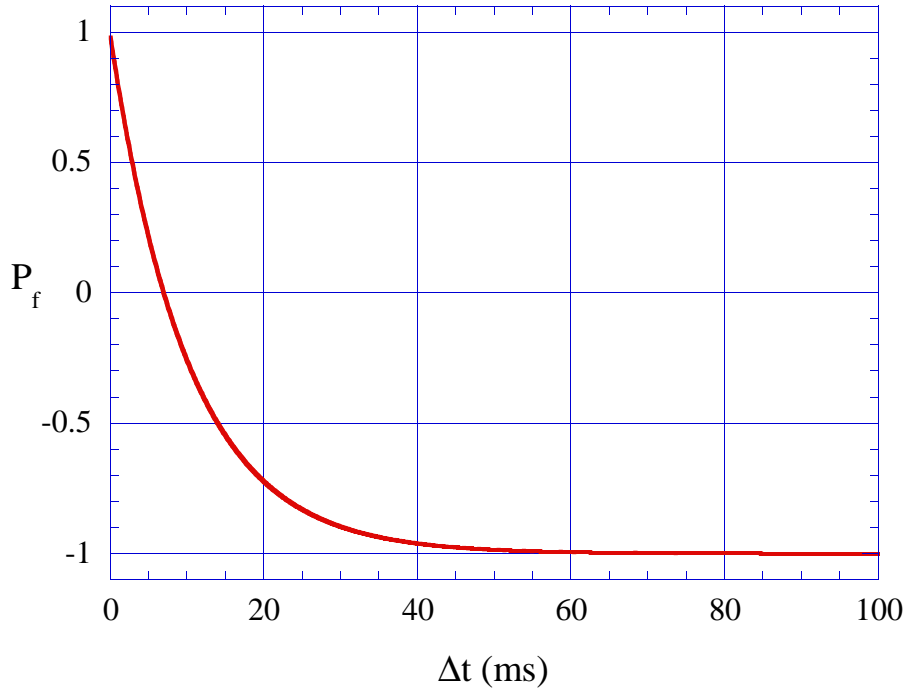


Figure II.3: Beam polarization after crossing an rf depolarizing resonance vs. ramp time

resonances cannot be totally isolated, and the frequency range cannot be infinite. Thus, the actual shape of a spin-flipping curve may not agree with the Froissart-Stora formula prediction, which is shown in Figure II.3. To maximize the spin-flip efficiency

$$\eta = \frac{-P_f}{P_i}, \tag{II.71}$$

the parameters ϵ , Δf , and Δt must be carefully adjusted.

CHAPTER III

EXPERIMENTAL APPARATUS

III.1 Introduction

Our spin-flipping experiments were done at the Indiana University Cyclotron Facility Cooler Ring during 1997-1998. Much of the apparatus used in these experiments was described in earlier papers [9, 10, 11, 12, 13, 14, 15, 16, 17, 18, 19, 20, 21, 22, 23, 24, 25, 26, 27, 28, 29]. The layout of IUCF during that period is shown in Figure III.1.

The polarized protons from the ion source were first accelerated in the Injector Cyclotron and next in the Main Cyclotron. The spin precession " θ "-solenoid rotated the injected beam polarization direction to match it with the SSD in the Cooler Ring. We monitored this injected beam polarization using the Beam Line 3 (BL3) polarimeter. Then, the beam was injected and stacked in the Cooler Ring for 10 to 30 seconds to achieve a high beam current.

The stored beam's polarization was measured using a carbon skimmer target polarimeter in the Cooler Ring's A region. The polarization direction of the injected beam was reversed every injection cycle to reduce the systematic error in this polarization measurement.

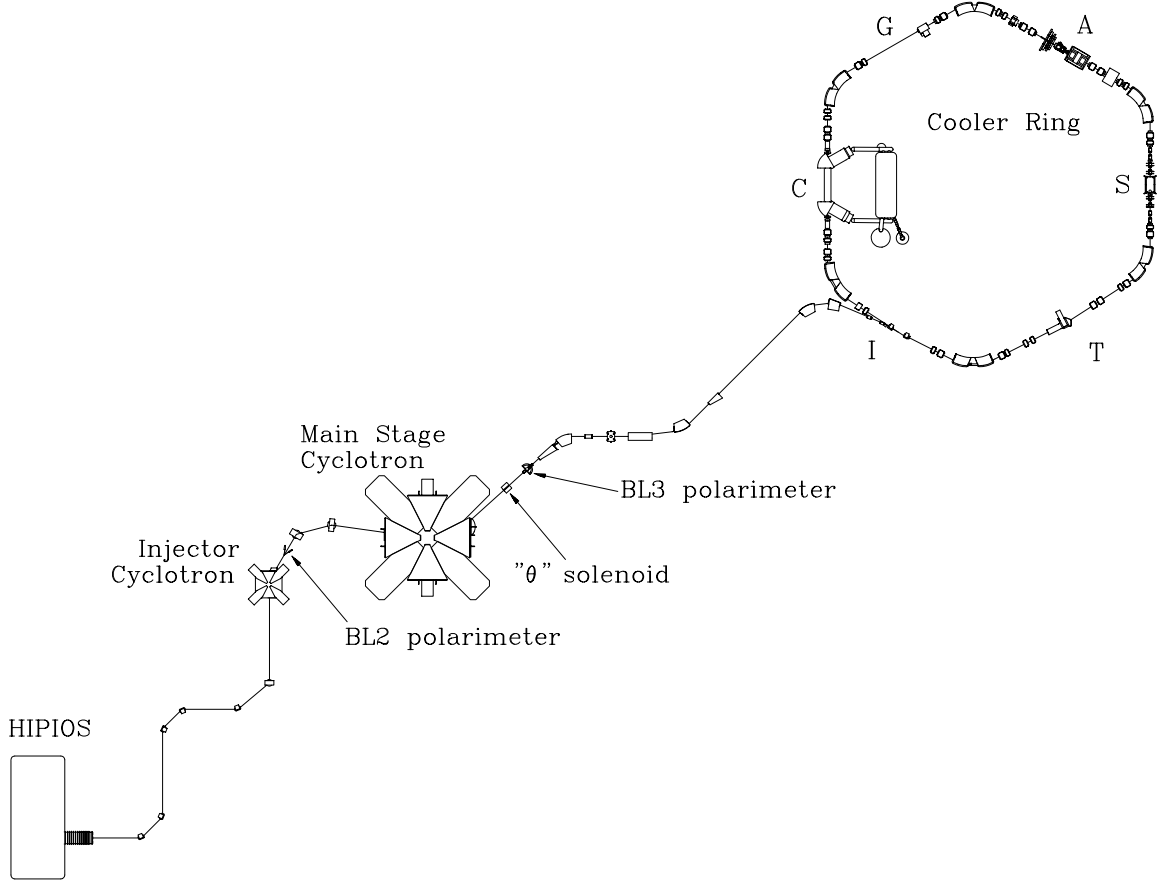


Figure III.1: Indiana University Cyclotron Facility circa 1997-1998.

III.2 Beam Acceleration in Cyclotrons and Polarization Rotation

The polarized proton beam was produced by the High Intensity Polarized Ion Source (HIPIOS) [30]. Its 20 keV polarized protons were accelerated in the Cockroft-Walton pre-accelerator to 600 keV and transported to the Injector Cyclotron, where they were accelerated to 15 MeV and then transported to the Main Stage Cyclotron, which accelerated the beam to 104.1 MeV.

The beam polarization emerging from the polarized ion source was vertical to match the field direction in the cyclotrons. However, with a full Siberian snake present in the Cooler Ring, the SSD was horizontal everywhere in the Ring. To match the injected polarization direction with this horizontal SSD, the vertical polarization

was rotated through 90° into the horizontal plane in the “ θ ” solenoid magnet, which required about 33.1 Amps for this 90° rotation at 104.1 MeV.

III.3 Polarized Beam Injection into the Cooler Ring

The polarized beam was stack-injected using: a Lambertson septum magnet in the middle of the Cooler Ring’s I section; a pair of fast-rise kickers at either end of this section; and a pair of RF cavities, as shown in Figure III.2.

When the two kickers were on, the injected beam entered the ring and circulated around the **injection orbit**, which passes through the septum and is slightly different

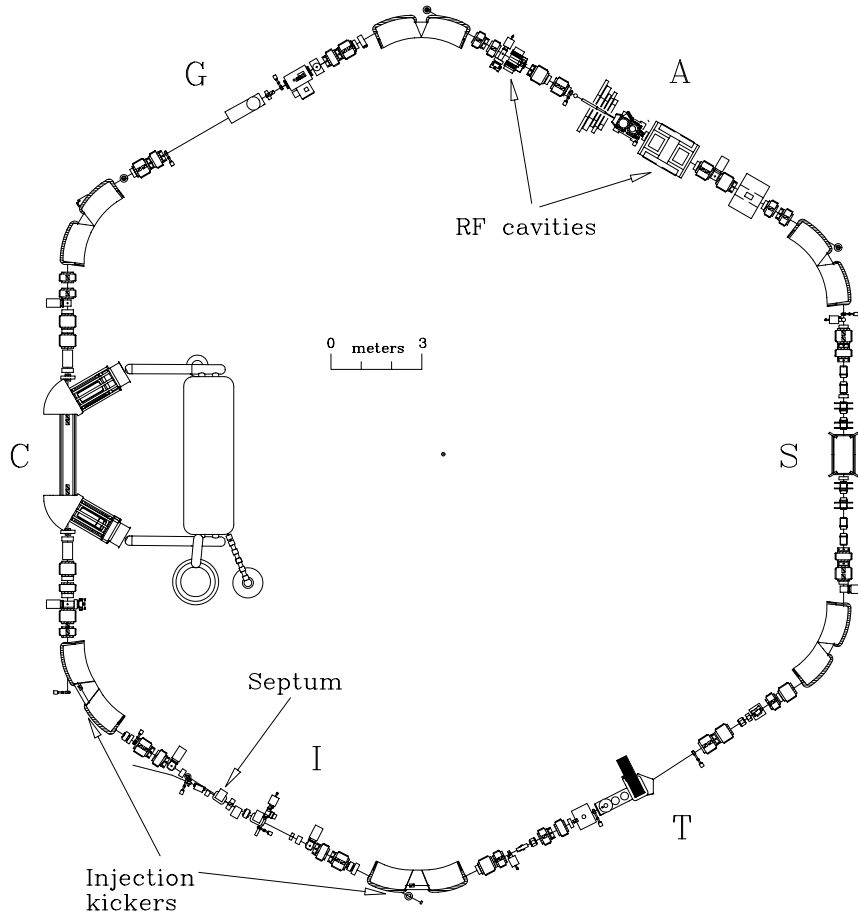


Figure III.2: Injection hardware in the Cooler Ring

from the **stored beam orbit** as shown in Figure III.3. Abruptly turning off the kickers then moved the injected beam into the **stack orbit** in the field-free region of the Lambertson magnet.

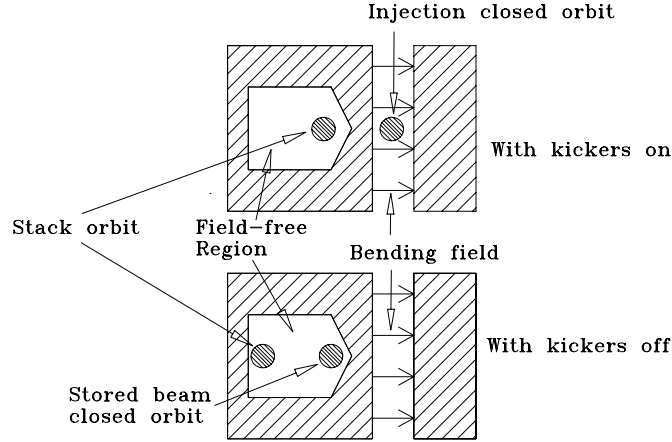


Figure III.3: Beam positions in the Lambertson septum

The injected protons had a slightly higher energy than the stored protons; thus the **stack orbit's** radius was slightly larger than the **stored beam orbit**. The rf cavities were then used to quickly decelerate the newly injected protons and thus move them to the **stored beam orbit**.

The Cooler Ring's electron cooling system was then used to reduce the protons' momentum spread by injecting into the Cooling straight section C a nearly mono-energetic beam of electrons, whose velocity matched the stored protons' velocity. Because of their much lower mass, the electrons had a much lower energy spread and thus were "cooler" than the more massive protons. The "hot" protons then interacted with the "cold" electrons, which reduced the protons' momentum spread [31]. The "heated" electrons were then removed from the Cooler Ring.

The protons were cooled for many turns with the injection kickers off until they were cooled such that their momentum spread was about $\Delta p/p = 2 \cdot 10^{-4}$. This injection and cooling process was repeated about every 150 *ms*, until the desired beam current was stored.

This stacking injection resulted in bunched beam currents of up to $500\ \mu A$ in the Cooler Ring by using the DC proton beam from the cyclotrons. However, our full Siberian snake caused some beam aperture difficulties (see Section III.5), and limited the stored beam current in the Cooler Ring to about $10\ \mu A$; fortunately this was adequate for a $\pm 2\text{-}3\%$ measurement of the polarization in about 15 minutes.

III.4 The Cooler Ring

The full layout of the Cooler Ring is shown in Figure III.4. The Ring's circumference is about 82.78 m and its maximum accelerated proton beam energy is about 500 MeV; the Ring's maximum injection energy is determined by the Main

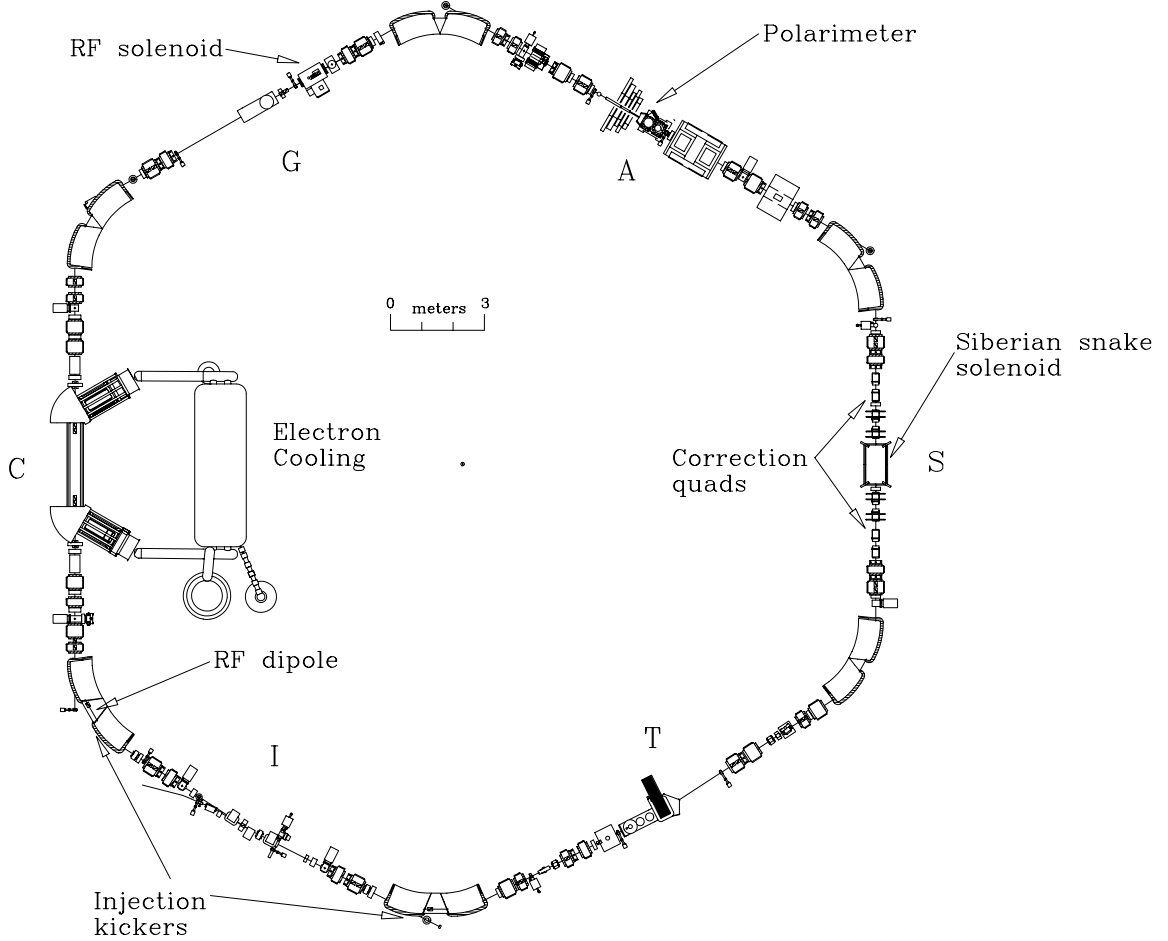


Figure III.4: The Cooler Ring

Stage Cyclotron's maximum energy, which is about 200 MeV. The Cooler Ring is a strong-focusing synchrotron with a 3-fold symmetry and six $\pi/3$ bends between its six straight sections; it has a FOFDOD quadrupole lattice. The Ring's main quadrupoles are organized into several "combos" with separate power supplies; this allows the Cooler Ring's betatron tunes to be varied. The accelerating rf field is provided by the larger of the two rf acceleration cavities, which were mentioned in Section III.3. This cavity, which is called the PPA cavity, generated the rf acceleration field and provided beam bunching by running at an appropriate harmonic of the beam's circulation frequency f_c . The smaller rf cavity, called the MPI cavity, was only used during the injection; its frequency was equal to f_c .

The Cooler Ring's six straight sections accommodate a large amount of experimental hardware for both nuclear physics and accelerator physics experiments. The **injection section I** was described in detail in Section III.3.; its upstream injection kicker magnet was also used as an rf dipole for our experiment. The T section is dedicated to nuclear physics experiments, while the Siberian snake solenoid and its eight correction quadrupoles are installed in the **snake section S**. The polarimeter is located in the A section, along with some nuclear physics experiments. The G section accommodates the RF solenoid and a small polarized hydrogen target, used in three-body forces studies. The Electron Cooling System is installed in the **cooler section C** as discussed in Section III.3.

III.5 The Siberian Snake

A Siberian snake can be constructed of either a single solenoid magnet or a series of dipole magnets with different field orientations; however, a solenoid is most suitable for low energies. Although its $\int B \cdot dl$ is energy dependent, it does not create any orbit excursions, which can be very large inside a dipole snake at low energies. Moreover, for energies below 500 MeV, a solenoidal snake containing a superconducting solenoid

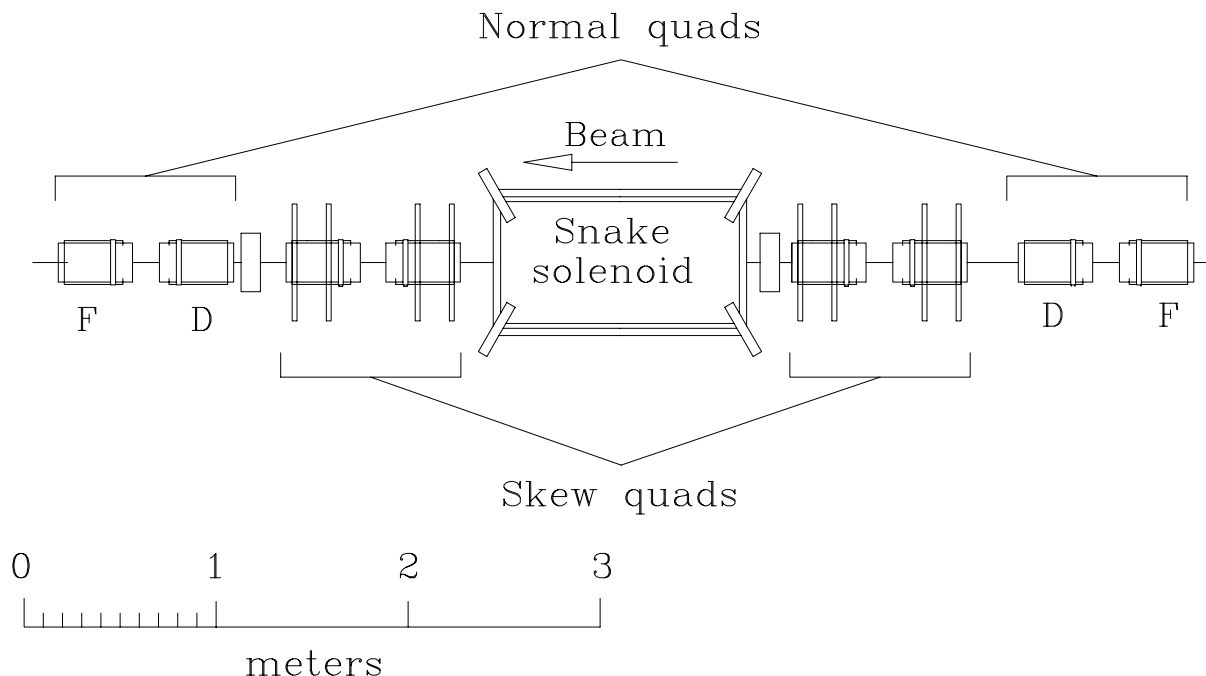


Figure III.5: The Siberian snake

can be much shorter than a dipole snake. Thus, at the 500 MeV IUCF Cooler Ring, a superconducting solenoid magnet was used as our snake.

One unfortunate feature of a high-field solenoid is that it causes strong beam focusing and strong betatron coupling. To allow successful beam operation, these two effects were compensated using a set of 8 correction quadrupoles. The Siberian snake's solenoid and the quadrupoles are shown in Figure III.5.

The eight correction quadrupoles consisted of two antisymmetric focusing-defocusing pairs of normal quadrupoles far from the solenoid and two antisymmetric pairs of skew quadrupoles near the solenoid. Note that a skew quadrupole is a normal quadrupole, which is rotated by some angle about its axis. The normal quadrupoles' strengths were set to cancel the solenoid's focusing of the beam, while the skew quadrupoles' angles and currents were set to cancel the betatron coupling caused by the solenoid. However, we could not completely cancel these two effects; this caused a lower beam intensity in the presence of the full snake.

The superconducting solenoid magnet had $N = 13,450$ turns and could operate

at a maximum current $I = 171$ Amps, where its maximum field integral is:

$$\int B \cdot dl = \mu_0 N I = 2.90 \text{ T} \cdot \text{m}, \quad (\text{III.72})$$

where $\mu_0 = 4\pi 10^{-7} \text{ T} \cdot \text{m} \cdot \text{A}^{-1}$. For a 100 % Siberian snake ($s = 1$) at 104.1 MeV, where the proton's momentum is 0.454 GeV/c, Equation II.38 indicates that the required field integral is:

$$\int B \cdot dl = 3.752 \cdot 1 \cdot 0.454 = 1.70 \text{ T} \cdot \text{m}, \quad (\text{III.73})$$

A schematic drawing of the Siberian snake's superconducting solenoid, used during 1997-1998, is shown in Figure III.6. The solenoid consists of a 122 cm long, 64 cm

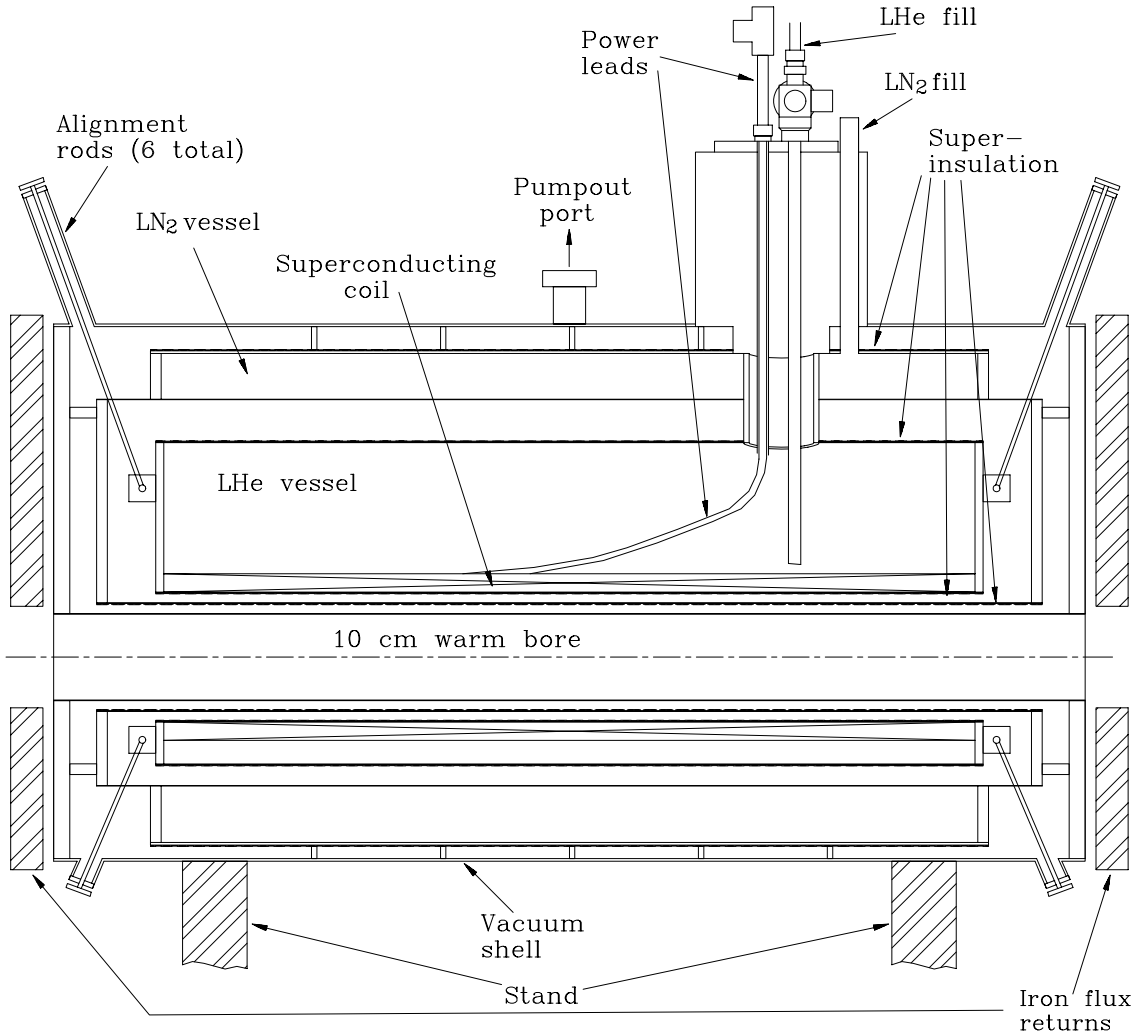


Figure III.6: The Siberian snake solenoid layout

O.D. stainless steel vacuum shell with a 10 cm warm bore, a 50 liter liquid nitrogen tank, and an 80 liter liquid helium tank which contains the solenoid coil. The liquid helium vessel is supported by six alignment rods. All outer surfaces of the liquid nitrogen and liquid helium tanks are covered with about 10 layers of superinsulation. The instrumentation rack on the top of the vacuum shell houses the liquid helium and liquid nitrogen fill ports, and the current leads. These power leads are cooled by the flow of very cold helium gas, evaporating from the liquid helium tank. The solenoid is enclosed in a flux return box made of a 4 cm thick iron.

To ensure good stability of the snake strength and thus the spin tune during the run, we used a very stable EMI Corp. EMS 20-250 DC power supply for our snake solenoid; the supply's current stability was about $\pm 0.01\%$. The power supply could be controlled both locally and remotely; we used the remote mode to adjust the current during the run.

The superconducting solenoid could operate for approximately 16 hours between refills of liquid helium. Since the snake solenoid could not operate in the persistent mode, each refill required ramping down the solenoid current. After filling the solenoid with helium, it was necessary to ramp it back up and then attempt to reset the current to its original value. The snake solenoid's current was measured and set using a high precision DC current transformer (DCCT). The output voltage of the DCCT, which was directly proportional to the snake's current, was precisely measured by a Keithley 155 nulling voltmeter; the precision of this current measurement was about 10 p.p.m.

III.6 The RF-Solenoid

An rf resonance can be created by a magnet, whose field amplitude oscillates at an "rf" frequency in the megahertz range. Such an rf magnet could be either an rf dipole or an rf solenoid. Here, as with a Siberian snake, a solenoid has several advantages

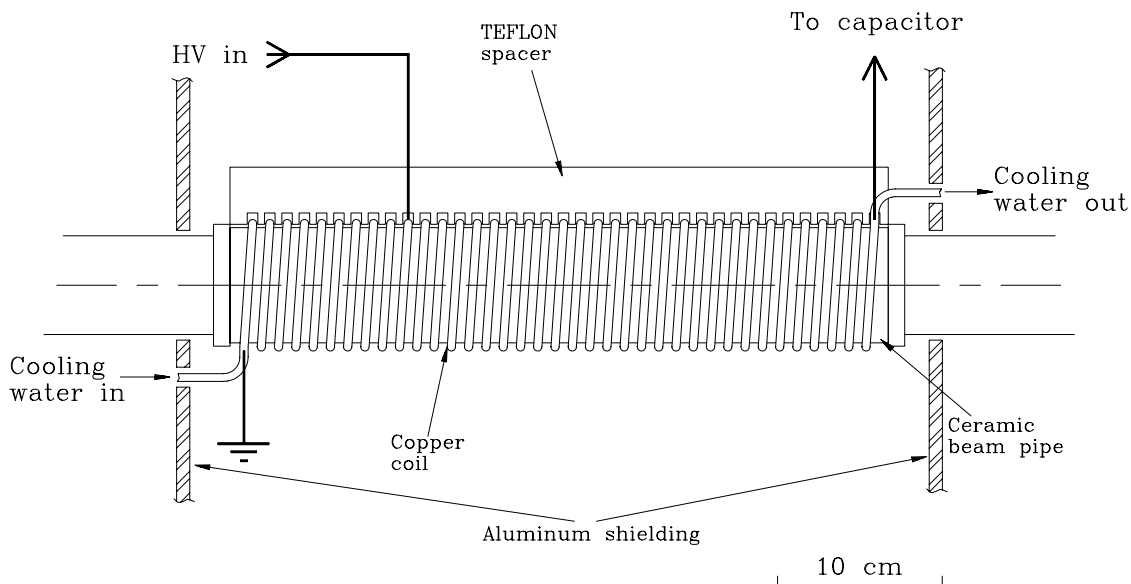


Figure III.7: RF solenoid

at low energies. Although its strength is reduced by the Lorentz contraction of its longitudinal $\int B \cdot dl$, this longitudinal field does not affect the beam motion. An rf dipole, at a frequency near any integer multiple of the horizontal or vertical betatron frequencies, could significantly increase the transverse beam oscillations, which could destroy the beam.

The rf solenoid magnet, which was installed in the Cooler Ring, is shown in Figure III.7 [28]. It consists of a 37-turn water-cooled copper coil, wound around a 3" O.D. ceramic beam pipe, with 3 Teflon combs to separate the adjacent turns of the coil, and an aluminum housing, which shields the surrounding equipment and nearby radios from the solenoid's rather strong rf radiation.

A diagram of the rf solenoid's electronic components is shown in Figure III.8. The rf signal for the rf solenoid was initially generated using a Hewlett-Packard HP8656 frequency synthesizer; a typical signal's frequency was about 2.2 MHz and its amplitude was typically set to +6 dBm, which corresponded to about 0.9 V peak-to-peak voltage with the rf synthesizer's 50 Ohms load. This signal's amplitude was then

stabilized by an automatic level controller box (ALC), which made the rf solenoid's voltage independent of frequency by measuring the rf field with a pick-up loop inside the rf solenoid and then adjusting the amplification to keep the field constant. The signal was then amplified by an ENI Inc. A150 rf power amplifier. The output of the A150 was applied to the grid of the EIMAC 4CW 10,000A tetrode amplifier tube, which produced an rf voltage of up to about 7 kilovolts.

We ran the rf synthesizer in a fixed frequency mode for our rf resonances studies. For the spin-flipping studies, the rf synthesizer's frequency was modulated to produce a frequency ramp around the 2.2 MHz central frequency. A ramp's typical range Δf

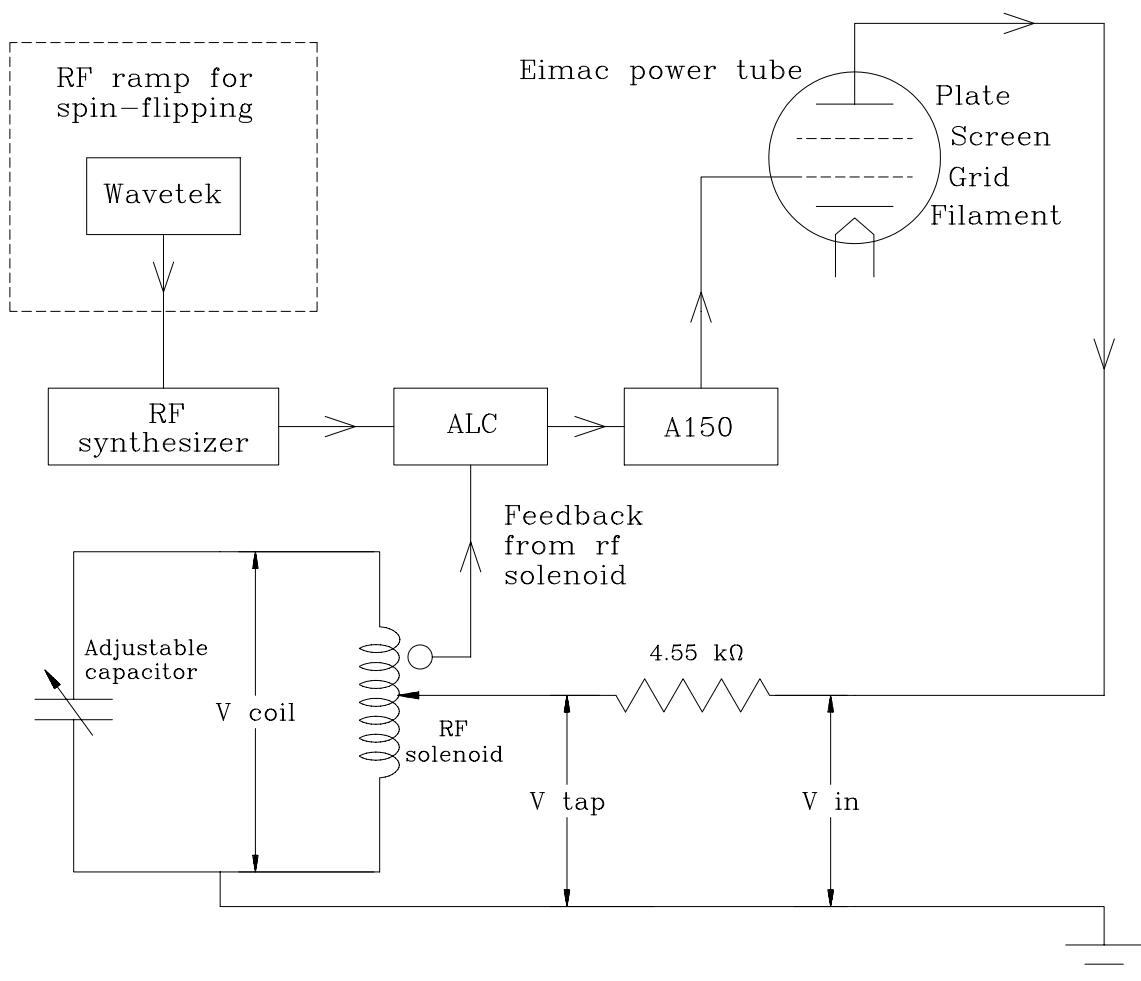


Figure III.8: RF solenoid's electronics

was about ± 6 kHz, its time duration Δt was between 1 and 1000 ms. This modulation was produced by a Wavetek model 90 arbitrary waveform generator.

To achieve a high rf magnetic field with this 37-turn solenoid, a 10-1000 pF vacuum variable capacitor was wired in parallel with the solenoid coil to form an LC resonant circuit. The rf voltage V_{in} from the EIMAC power amplifier tube was applied to the coil's tap point through a $4.55\text{ k}\Omega$ resistor to increase the quality factor of the LC resonance circuit; the typical Q-value at 2.2 MHz was about 200. The tap point was located at approximately 1/4 of the length of the coil to match the input impedance of the resonance circuit to the output impedance of the tube. Thus, the total rf voltage amplitude across the solenoid V_{coil} was about 4 times higher than the applied voltage V_{tap} . We ran at the maximum rf voltage across the solenoid of about 6 kV amplitude; its maximum longitudinal $\int B \cdot dl$ was about 1.6 T·mm.

III.7 The RF-Dipole

To study rf depolarizing resonances with an rf dipole, we used one of the Cooler Ring's injection kicker dipoles; the kicker magnet is shown in Figure III.9. It is a ferrite magnet 8 cm high by 24 cm wide by 40 cm long with a one-turn coil; it fits inside a 26 cm O.D. stainless steel vacuum chamber with a 1.6 mm wall thickness.

A diagram of the rf dipole's electronics is shown in Figure III.10. Since, during each Cooler Ring cycle, the ferrite dipole had to be used as both an injection kicker and an rf dipole, it was necessary to switch the dipole's input between the kicker power supply and the rf power supply. Therefore, we installed two pneumatic rf switches with a 100 msec switching time. During injection, the switches were in the inner position, and the kicker power supply pulses were applied to the dipole. At the start of the flattop, the switches were turned to the outer position, and the output of an A150 rf power amplifier was connected to one lead of the dipole. The other lead was terminated with a 50 Ohm resistor to match the output impedance of the

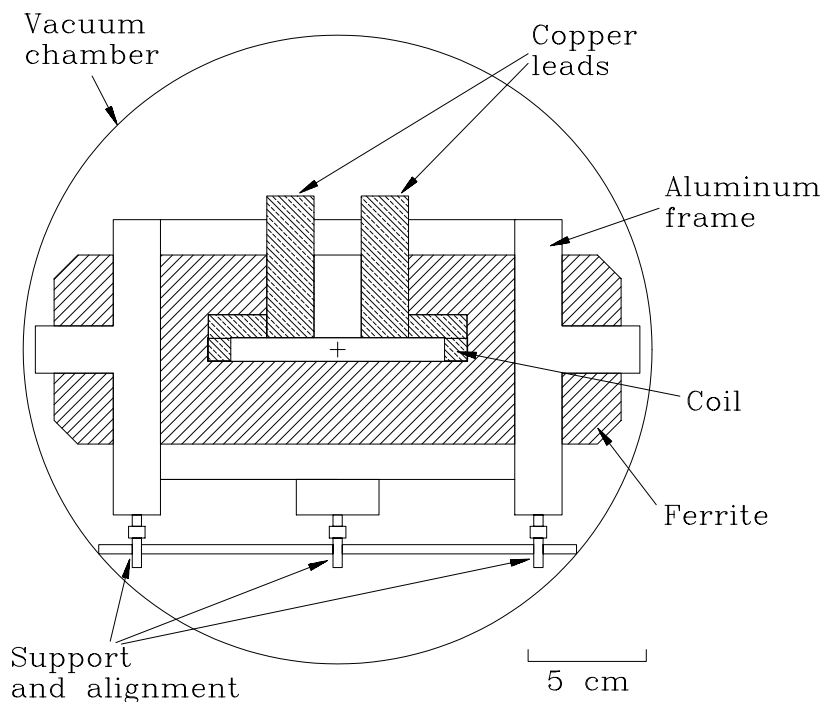


Figure III.9: RF dipole (beam view)

A150. The rf signal for the rf dipole was generated by the same rf synthesizer and ALC as was used for the rf solenoid. However, we did not use the EIMAC power amplifier, since its high-voltage output might have destroyed the $L = 4.1 \mu\text{H}$ ferrite dipole. Moreover, the rf dipole was not a part of a high-Q resonant LC circuit.

Unfortunately, we were not able to perfectly match the output of the A150 power

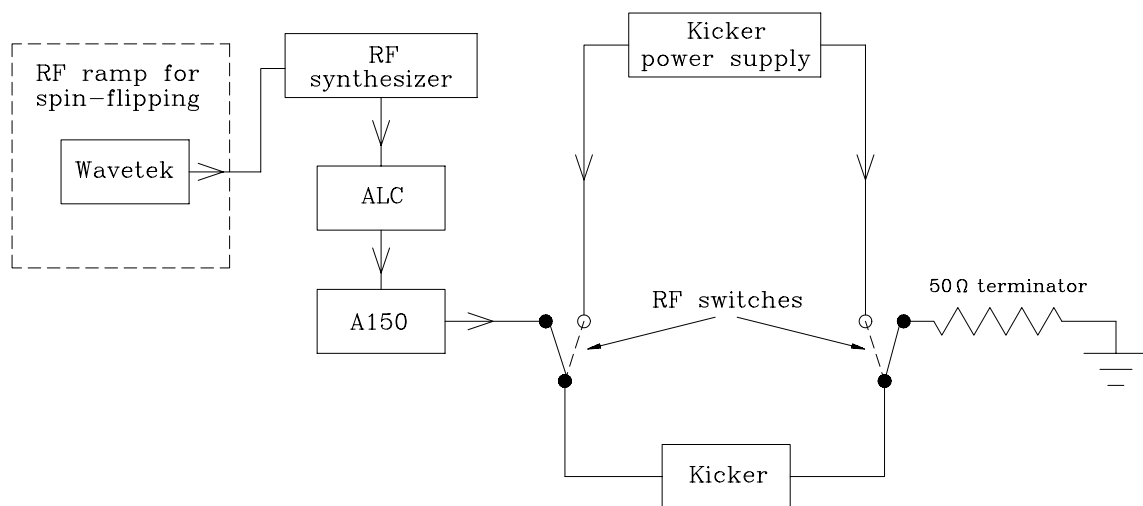


Figure III.10: RF dipole's electronics

amplifier and the input of the rf dipole. This mismatch, which was probably caused by the rf switches, significantly reduced the voltage across the dipole and consequently its resonance strength. The maximum r.m.s. voltage that we were able to reach was only about 23 V; this corresponded to an $\int B \cdot dl$ of about 0.03 T·mm.

III.8 Polarimetry

The proton beam polarization was monitored carefully during each stage of the beam acceleration. The initial polarization of the beam emerging from the Injector Cyclotron was measured by the BL2 polarimeter, which used the elastic scattering of protons on its ^4He gas target [32]. The analyzing power of $p + ^4\text{He} \rightarrow p + ^4\text{He}$ at the Beam-Line-2 energy of about 15 MeV was close to 1.0 for all angles.

The polarization of the beam extracted after acceleration by the Main Cyclotron was measured by the BL3 polarimeter [33], which is shown in Figure III.1. The BL3 polarimeter used a thin $0.5 \mu\text{g cm}^{-2}$ deuterated polyethylene film, and detected both the scattered protons and recoil deuterons at the angles of 73.6° and 37.8° , respectively, in the up-down and left-right directions. The analyzing power A_n varies with the incident protons' energy, with a typical value of about 0.6.

The Cooler beam polarization was measured by a carbon target polarimeter in the A region, which is shown in Figure III.11 [34]. It consisted of a 3 mm thick carbon skimmer target, a collimator and the detectors: two sets of wire chambers, u-v and x-y, and two sets of scintillators, F and E. The skimmer target was moved into the circulating beam with its feedback loop connected to the detector rate meter; an increased rate would slow the inward motion of the target, thus providing a uniform rate of data acquisition during the polarization measurements.

The polarization measurement was based on the asymmetry of 104.1 MeV protons elastically scattered on C^{12} with an average analyzing power of about 0.233. The trigger for an elastic event was provided by an F and E coincidence, while the orthogonal

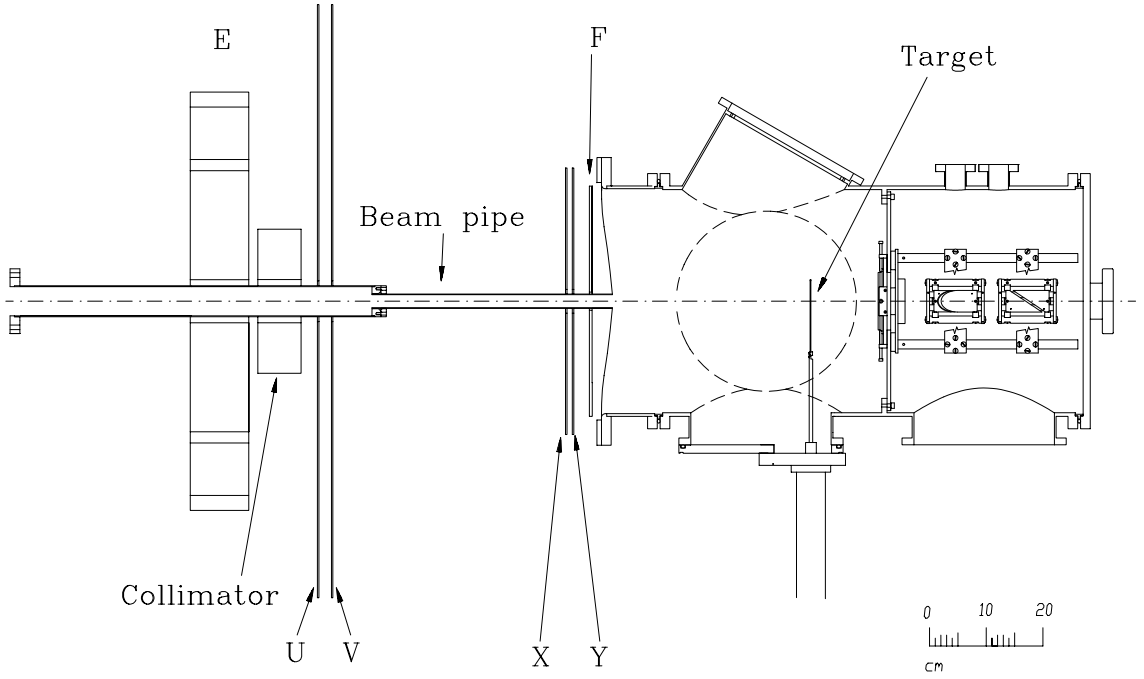


Figure III.11: Cooler polarimeter (top view).

wire chambers determined the tracks of scattered particles, ensuring that only events originating at the target were counted. These wire chambers also measured the angle θ between the scattered proton's track and the beam axis.

The elastic events were then divided, using software on-line analysis, into four regions (up, down, left and right) of $\pi/2$ each, and the vertical polarization was calculated by

$$P = \frac{1}{\bar{A}_n} \frac{\sqrt{N_{L\uparrow}N_{R\downarrow}} - \sqrt{N_{L\downarrow}N_{R\uparrow}}}{\sqrt{N_{L\uparrow}N_{R\downarrow}} + \sqrt{N_{L\downarrow}N_{R\uparrow}}}, \quad (\text{III.74})$$

where \bar{A}_n is the angle weighted averaged analyzing power, and $N_{L(R)\uparrow(\downarrow)}$ are the total numbers of events scattered into the *Left(Right)* detectors with the injected beam polarization *up(down)*. Similarly, the radial beam polarization was calculated from:

$$P = \frac{1}{\bar{A}} \frac{\sqrt{N_{U\uparrow}N_{D\downarrow}} - \sqrt{N_{U\downarrow}N_{D\uparrow}}}{\sqrt{N_{U\uparrow}N_{D\downarrow}} + \sqrt{N_{U\downarrow}N_{D\uparrow}}}, \quad (\text{III.75})$$

where $N_{U(D)\uparrow(\downarrow)}$ are the total numbers of events scattered into the *Up(Down)* detectors

with the injected beam polarization *up(down)*.

This algorithm of measuring the polarization eliminates most systematic errors, such as unequal efficiencies of different detectors and beam current fluctuations from cycle to cycle, which otherwise could cause false asymmetries. The main source of the measured polarization's systematic error is then the value of the analyzing power.

The analyzing power for proton-carbon elastic scattering was measured by several groups [35, 36, 37, 38] at many energies and angles. We determined the analyzing power using the parameterization of McNaughton *et al.* [38] for each momentum p_{lab} and laboratory scattering angle θ_{lab} :

$$A_n(\theta_{lab}, p_{lab}) = \frac{ar}{1 + bp_{\perp}^2 + cp_{\perp}^4}, \quad (\text{III.76})$$

where $p_{\perp} = p_{lab} \sin \theta_{lab}$, the momentum p_{lab} is in GeV/c , and the parameters a , b and c are given by

$$a = a_0 + a_1 p' + a_2 p'^2 + a_3 p'^3 + a_4 p'^4, \quad (\text{III.77})$$

$$b = b_0 + b_1 p' + b_2 p'^2 + b_3 p'^3 + b_4 p'^4, \quad (\text{III.78})$$

$$c = c_0 + c_1 p' + c_2 p'^2 + c_3 p'^3 + c_4 p'^4, \quad (\text{III.79})$$

where $p' = p_{lab} - 0.7 \text{ GeV}/c$, and the parameters a_i , b_i and c_i are given in Table III.1.

	0	1	2	3	4
a_i	5.3346	-5.5361	2.8353	61.915	-145.54
b_i	-12.774	-68.339	1333.5	-3713.5	3738.3
c_i	1095.3	949.50	-28012	96833	-118830

Table III.1: McNaughton *et al.*[38] parameterization coefficients for A_n , which are valid between 100 and 450 MeV

CHAPTER IV

EXPERIMENTAL RESULTS AND ANALYSIS

IV.1 Introduction

The results of four experimental runs of CE-69 [39] are discussed here. These include measurements of the locations and widths of snake rf depolarizing resonances using both the rf solenoid and the rf dipole; they also include spin-flipping studies using these rf magnets in the presence of a nearly-full Siberian snake.

For all four runs, a 104.1 MeV polarized proton beam was stored in the IUCF Cooler Ring; the circulation frequency f_c was $1,504,900 \pm 10$ Hz. The Ring's rf acceleration cavity operated at the sixth harmonic of f_c at a frequency of $9,029,400 \pm 10$ Hz.

The Siberian snake solenoid's current varied slightly from run to run around 103 A; this corresponded to a snake strength of approximately 1.02.

IV.2 RF resonances

In order to spin-flip a stored polarized beam using an rf depolarizing resonance, the resonance's location and width must be first determined; then the rf frequency ramp's central frequency and frequency range Δf can be chosen. With a nearly-full Siberian snake in the Cooler Ring, the spin tune was very close to $1/2$, as given by Equation II.63. Recall that Equations II.66 and II.67 indicate that rf depolarizing

resonances should then be found in closely spaced pairs around half-integer values of the circulation frequency f_c . In our experiments we mainly studied the rf depolarizing resonances near $f = f_c(2 - \nu_s)$. At 104.1 MeV, where $G\gamma = 1.9918 \simeq 2$, Equations II.66 and II.67 simplify to:

$$f_l \simeq f_c(1.5 - \delta s/2) \quad (\text{IV.80})$$

and

$$f_u \simeq f_c(1.5 + \delta s/2), \quad (\text{IV.81})$$

where $\delta s = |1 - s|$ is the amount by which the snake strength s differs from a full snake.

The exact location of these "upper" and "lower" resonances depends strongly on the snake strength s , which is proportional to the snake solenoid's current, as defined by Equation III.39. As given by Equation II.68, with a snake strength of about 1.02, the two resonances centered around $1.5f_c$ would be separated by about $\delta f \simeq 30$ kHz. This ensured that there was no overlapping between the upper and lower resonances.

IV.2.1 Experimental procedure

For the rf resonance mapping, the horizontally polarized proton beam was injected into the Cooler Ring, where it was stored and cooled. The rf solenoid or the rf dipole was turned on at a fixed frequency about 0.5 second after the start of the flattop. The data acquisition system was then turned on; then the target was moved into the beam and the polarization measurements were started. The rf magnet remained on throughout the flattop. At the end of the flattop, the data acquisition was turned off, then the rf magnet was turned off, and the beam was kicked out of the Ring using one of the injection kickers. A typical timing pattern of the rf magnets, detectors and data acquisition for an rf resonance mapping run is shown in Table IV.1.

We first operated the rf solenoid at its maximum strength to find the location of

Timing for:	Time ON (sec)	Time OFF (sec)
Flattop	0.000	30.000
RF solenoid (dipole)	0.600	29.950
Wire chambers	1.000	29.900
Target	1.600	29.900
DAQ	1.600	29.900

Table IV.1: Typical electronics timing for rf depolarizing resonance study with a 30 second flattop.

the rf depolarizing resonance. We varied the rf solenoid's frequency in 1 kHz steps around the expected position of the resonance; if the resonance was observed, then we took another set of data points with 1 kHz steps halfway between the first set of points; additional points were then taken near the resonance to better map it. Sometimes, the resonance was not found in the first set of points; we then scanned the regions above and below the expected position with the 1 kHz steps until a depolarization was observed.

This knowledge of the exact location of the rf resonance was used in subsequent rf dipole studies; the rf dipole's resonance would otherwise be relatively hard to find, because it was a much weaker magnet.

IV.2.2 Data and Analysis

Figure IV.1 shows the rf solenoid depolarizing resonance data for each of the four experimental runs. On each graph, the radial beam polarization is plotted against the rf solenoid's frequency. Note the different central resonance frequency for each run; this was due to slightly different snake solenoid currents.

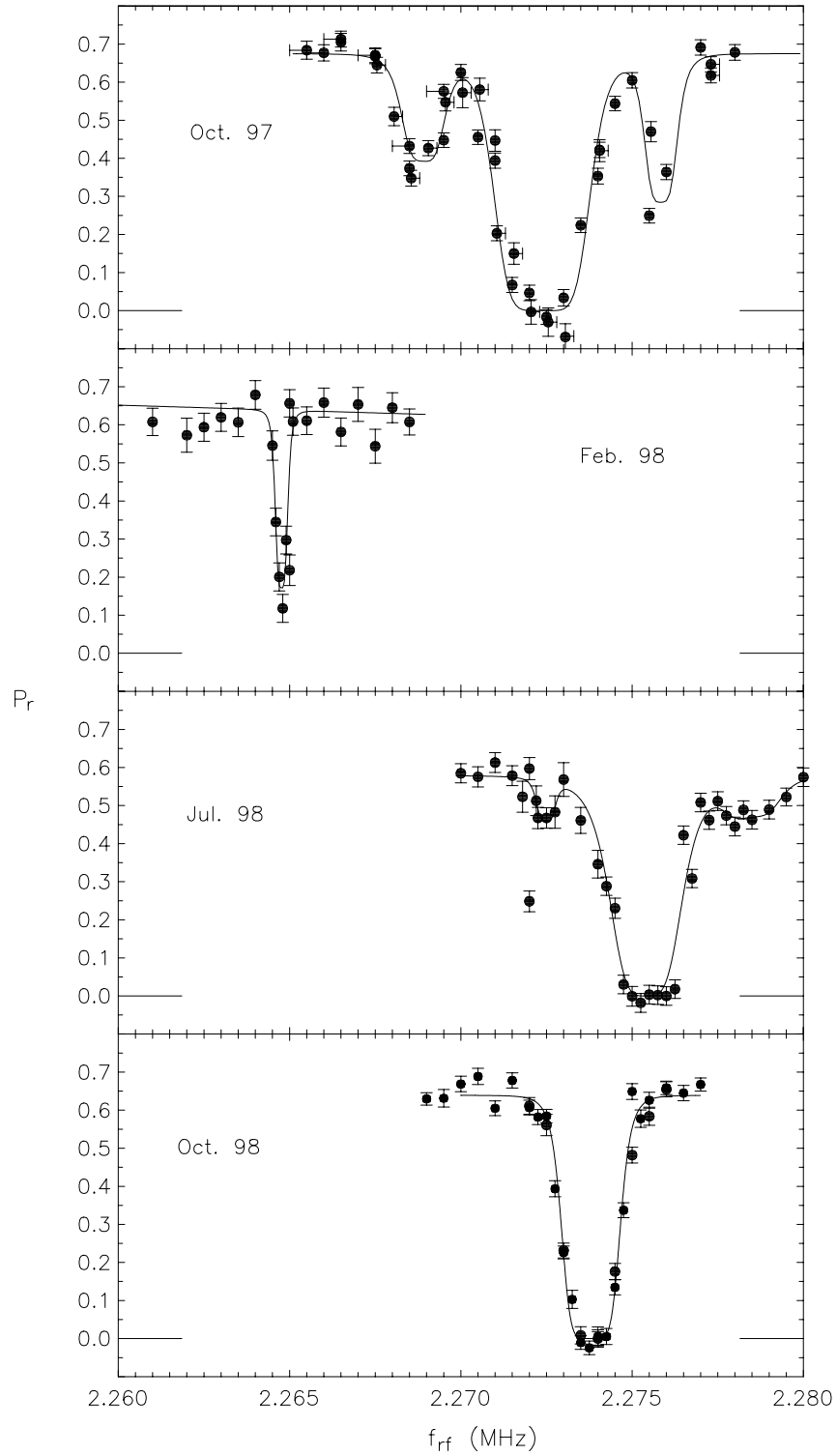


Figure IV.1: RF solenoid depolarizing resonances. The measured radial beam polarization at 104.1 MeV is plotted against the frequency of the rf solenoid.

In the July 1998 run we also used the rf dipole to create an rf depolarizing resonance; the experimental data is shown in Figure IV.2.

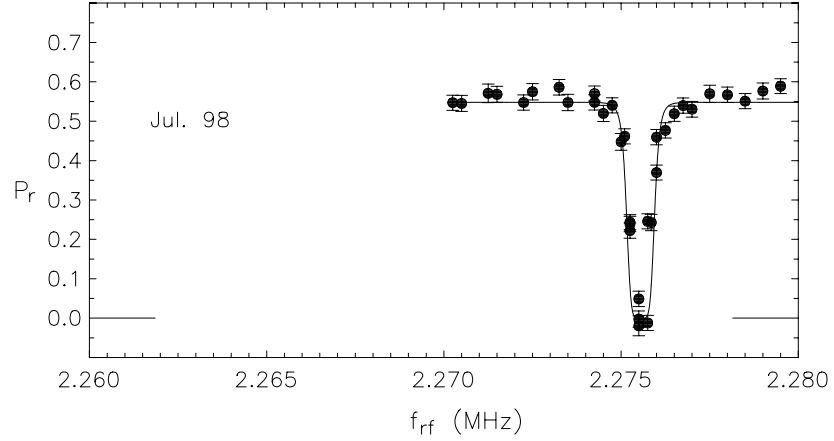


Figure IV.2: RF dipole depolarizing resonance. The measured radial beam polarization at 104.1 MeV is plotted against the frequency of the rf dipole.

We fit the rf depolarizing resonance's data in Figures VI.1 and VI.2 using second-order and higher-order Lorentzians:

$$P = P_0 \frac{(f - f_r)^{2n}}{(f - f_r)^{2n} + (w/2)^{2n}}, \quad (\text{IV.82})$$

where n is the order of the Lorentzian, P_0 is the full polarization, f_r is the resonance's central frequency, and w is the resonance's FWHM width (full-width at half-maximum)).

Note that two synchrotron sideband resonances were clearly present in the October 1997 and July 1998 data [25]; we fit them using higher-order Lorentzians with a variable depth:

$$P = P_0 \left(d_{sync} \left(\frac{[f - (f_r \pm f_{sync})]^{2n}}{[f - (f_r \pm f_{sync})]^{2n} + (w_{sync}/2)^{2n}} - 1 \right) + 1 \right), \quad (\text{IV.83})$$

where n is the order of the Lorentzian, P_0 is the initial polarization, d_{sync} is the synchrotron sideband's depth, f_r is the main resonance's central frequency, determined by fitting the main dip, f_{sync} is the sideband's central frequency with respect

Run date	Oct. 97	Feb. 98	July 98 (sol.)	July 98 (dip.)	Oct. 98
f_{res} (MHz)	2.27237	2.26477	2.27541	2.25549	2.27379
w (Hz)	2890	387	2260	636	1810
Lorentzian order	3	1	2	3	3
f_{sync}^+, f_{sync}^- (Hz)	3470, 3370	-	3075, 2924	-	-
w_{sync}^+, w_{sync}^- (Hz)	1030, 1360	-	1840, 606	-	-
d_{sync}^+, d_{sync}^-	0.45, 0.33	-	0.18, 0.19	-	-
Sync. sideband Lorentzian order	2, 2	-	2, 3	-	-

Table IV.2: Locations and widths of rf depolarizing resonances at 104.1 MeV.

to the main resonance's frequency, while the "+" and "-" signs represent the higher-frequency and lower-frequency sidebands, respectively, and w_{sync} is the sideband's FWHM width. These parameters for each graph are summarized in Table IV.2.

Note that, in Figure IV.1, the frequencies of some October 1997 data points were shifted by the amounts indicated by the single horizontal error bars. During the data taking, the snake solenoid was twice refilled with liquid helium; the solenoid's current could not be exactly reproduced after each fill, which resulted in a slightly different snake strength for each fill. This change in solenoid current of typically 0.02% caused a small change of the resonance's position for each fill; the frequencies of the data points are shifted on the graph to account for this change.

IV.3 RF depolarizing resonance widths

As mentioned in Section II.4, the measured widths of these rf depolarizing resonances was usually much larger than the simple single-particle model [28] prediction.

For an rf solenoid, this model predicts:

$$w_{th}^{sol} = f_c \epsilon^{sol} = f_c \frac{(1 + G)e \int B_{rf}^{sol} \cdot dl}{2\pi\gamma m_p v}, \quad (\text{IV.84})$$

where f_c is the circulation frequency, B_{rf}^{sol} is the r.m.s. rf magnetic field, while γ and v are the proton's Lorentz factor and velocity respectively. At the 6 kV maximum rf voltage across our rf solenoid, its $\int B_{rf}^{sol} \cdot dl$ was about 1.35 T·mm; then Equation IV.83 predicts an rf depolarizing resonance's width of about 600 Hz at 104.1 MeV.

However, as indicated in Table IV.2 and Figure IV.1, the measured resonances widths were usually about 2 kHz; the only exception was the February 1998 run, when the measured width of 387 Hz was somewhat closer to the theoretical value.

For an rf dipole, a similar formula [28] yields for the resonance width:

$$w_{th}^d = f_c \epsilon^d = f_c \frac{Ge \int B_{rf}^d \cdot dl}{2\pi m_p v}. \quad (\text{IV.85})$$

At our 23 V maximum r.m.s. voltage across the dipole, its $\int B_{rf}^d \cdot dl$ was about 0.03 T·mm, which gives a predicted resonance width of only about 110 Hz. As indicated in Table IV.2 and Figure IV.2, the width observed in July 1998 was about 1 kHz.

To determine possible sources of this width broadening, we recently measured resonance widths at different conditions [10]. We found that the rf resonance's width depends strongly on the rf acceleration voltage, which drives the synchrotron oscillations of the beam protons' energy; with these rf acceleration cavities turned on, the rf depolarizing resonance width was about twice wider than with the rf cavities off. When the rf acceleration cavities were turned on at a high voltage of about 1.5 kV, the energy of the stored protons oscillated with a 4 kHz synchrotron frequency around the equilibrium energy [40]; the amplitude of these oscillations depended on the beam's momentum spread $\Delta p/p$, which was about $2 \cdot 10^{-4}$ with the electron cooling on. Because of these synchrotron oscillations, each proton's circulation frequency f_c and spin tune ν_s also oscillated with the same frequency of about 4 kHz and with amplitudes

$\Delta f_c/f_c$ and $\Delta \nu_s$ of approximately 0.02% each. This spread in f_c and ν_s resulted in some of the protons having an f_c and ν_s which satisfied the resonance condition; this could partially depolarize the beam even when the rf solenoid or the rf dipole was relatively far away from the resonance frequency, defined by Equation IV.79 or IV.80.

We also found that the measured rf depolarizing resonance width usually depended very weakly on the magnetic field strength of either the rf solenoid or the rf dipole. When the strength of each rf magnet was reduced by a factor of two, the measured rf resonance width only changed by about 5%. This indicates that the measured width of the rf depolarizing resonance was not dominated by the resonance's strength.

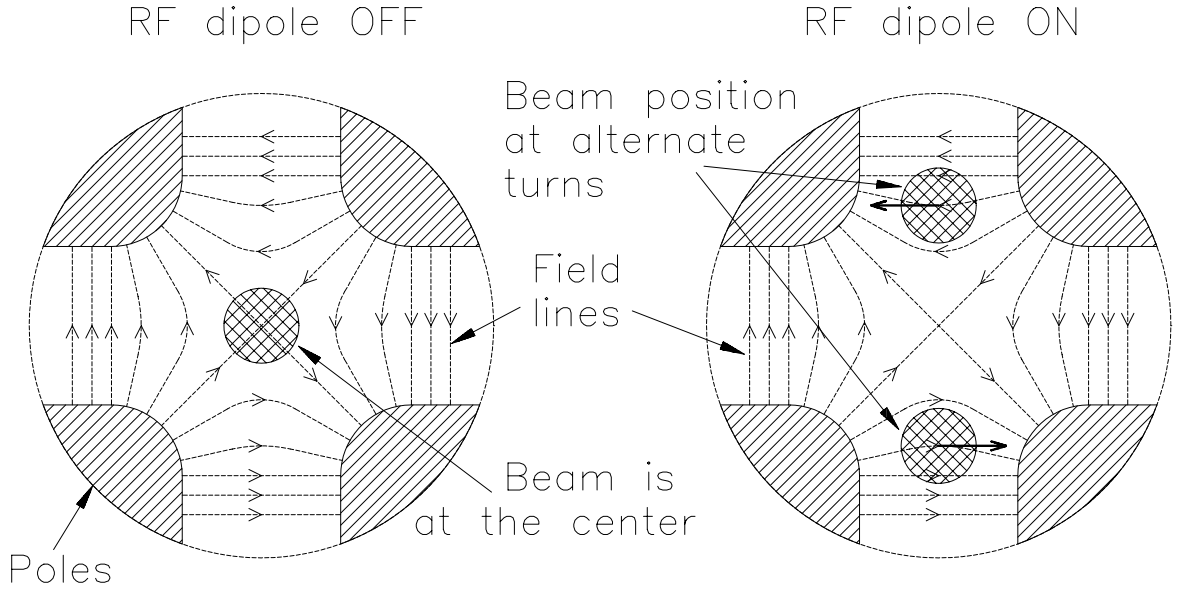


Figure IV.3: Possible rf dipole depolarizing resonance enhancement due to coherent betatron oscillations in a quadrupole.

An interesting mechanism involving coherent betatron oscillations was suggested [41] for the increase of an rf dipole's resonance width. An rf dipole with a horizontal magnetic field would increase the vertical betatron oscillations' amplitude which could be large if the rf dipole's frequency is near the vertical betatron frequency. Figure IV.3 shows such coherent betatron oscillations when the rf dipole frequency is a half-integer times the circulation frequency; the beam center's displacement is then opposite at

consecutive turns. The beam's protons would all then encounter horizontal magnetic fields of this quadrupole, which are indicated by solid arrows. In the protons' rest frame, these fields' horizontal $\int B \cdot dl$ would have the rf dipole's frequency ($1/2f_c$) and thus could effectively increase the resonance's strength. Such rf-dipole-induced coherent beam oscillations were successfully used to make a Brookhaven AGS intrinsic depolarizing resonance strong enough to spin-flip with no depolarization [42].

IV.4 Spin-flipping

We spin-flipped a stored horizontally-polarized proton beam using either the rf solenoid or the rf dipole by sweeping the magnets' frequency through the rf depolarizing resonance found earlier in the experiment. The main goal of our spin-flipping studies was to maximize the spin-flip efficiency η , defined by Equation II.70.

To maximize the efficiency of the spin-flip we varied the frequency ramp time Δt and the frequency ramp range Δf , while measuring the beam polarization after a spin-flip; these two parameters determine the resonance crossing rate $\Delta f / \Delta t$. According to the Froissart-Stora formula (Equation I.7), a slower rate of crossing the resonance yields a higher final polarization, and thus a higher spin-flipping efficiency η . To make the crossing rate $\Delta f / \Delta t$ slower, one can either increase the ramp time Δt or reduce the frequency range Δf .

Increasing the ramp time while holding Δf fixed is technically quite easy; this suggests that a very long Δt should allow an almost perfect spin-flip. However, our earlier experiments [18] found that at very long ramp times (greater than about 500 ms) this efficiency decreases. Thus, there may be an optimum setting for Δt , which gives the highest final beam polarization.

Varying the frequency range Δf , while holding Δt fixed, can change the spin-flip efficiency in two ways: by changing the crossing rate $\Delta f / \Delta t$ and by making the resonance crossing incomplete at narrow frequency ranges. The first mechanism

dominates when Δf is much wider than the resonance width w ; thus, to improve the spin-flipping efficiency one should decrease Δf , which reduces the resonance crossing rate. However, when the frequency range becomes smaller than the width of the resonance, the second mechanism becomes important. The rf magnet is then turned on and off at frequencies where the beam is already partially depolarized; this certainly reduces the final polarization after a spin-flip. Clearly, one should choose the optimum Δt and Δf to simultaneously minimize both of these efficiency-reducing mechanisms.

IV.4.1 Experimental procedure

During the spin-flipping studies, the experimental procedure differed slightly from the procedure used to map an rf resonance. After injecting, storing and cooling the beam, the Wavetek waveform generator (Figure III.8) was triggered and then the rf magnet was turned on; following the control signal from the Wavetek, the rf magnet then ran for about 10 ms at a frequency $f_r - \Delta f/2$. During a time Δt , the Wavetek ramp then linearly increased the rf magnet's frequency to a frequency above the resonance's central frequency f_r ; the Wavetek then kept the rf magnet at this frequency $f_r + \Delta f/2$ for the rest of the flattop.

IV.4.2 Spin-flipping by varying the ramp time

The location and width of the rf depolarizing resonance used for spin-flipping were first determined from a resonance mapping such as in Figure IV.1 and IV.2. We then set the frequency range Δf so that it completely bracketed the rf resonance by extending symmetrically on both sides by about two resonance widths; then we varied the ramp time Δt .

Figure IV.4 shows the results of spin-flipping using the rf solenoid by varying its ramp time; the measured radial beam polarization after a single spin-flip is plotted

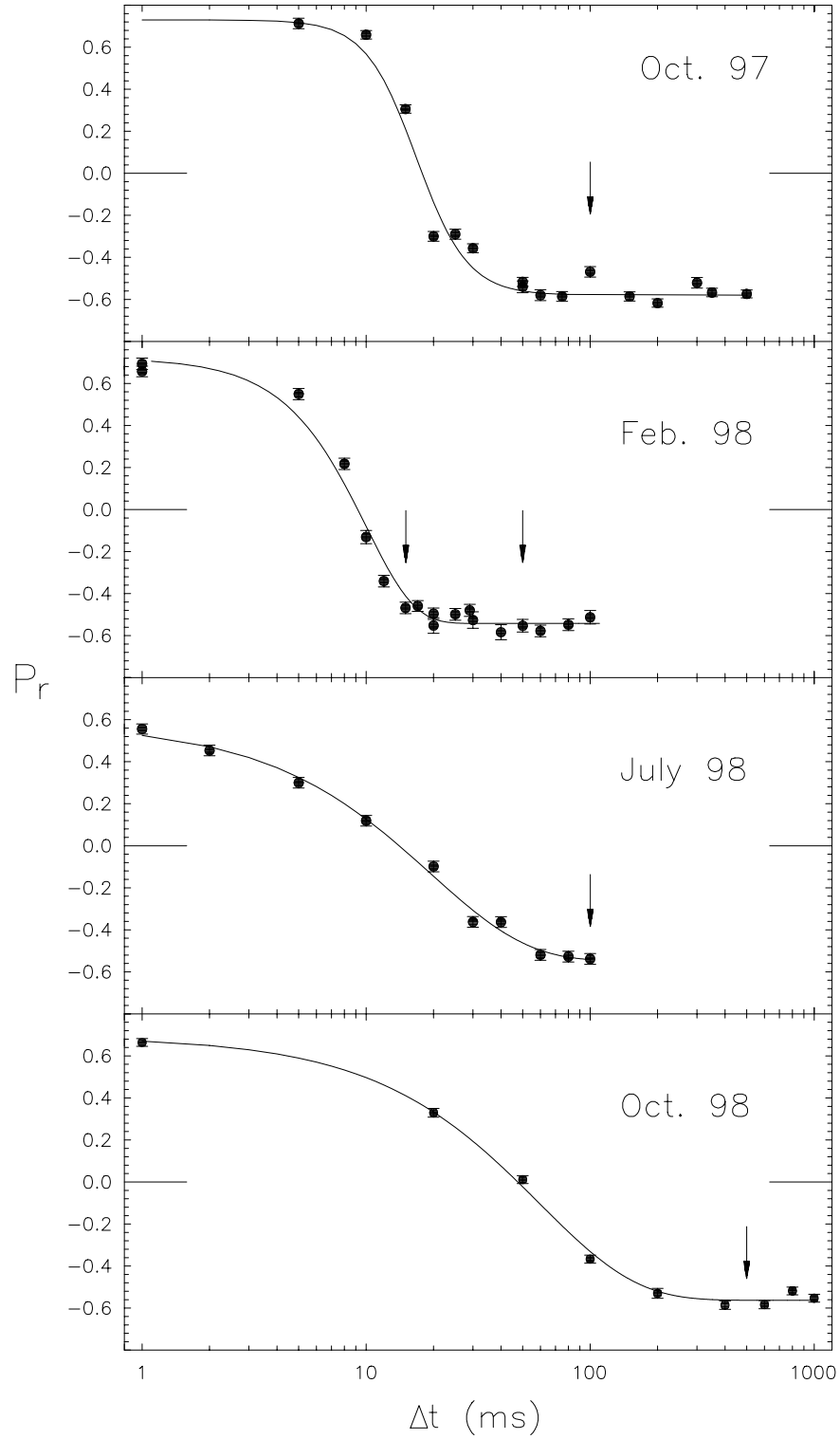


Figure IV.4: Spin-flipping while varying the rf solenoid's ramp time. The measured radial beam polarization at 104.1 MeV is plotted against the ramp time Δt . Arrows indicate the ramp times, used in spin-flipping while varying the frequency range, as described in Section IV.4.3.

against the ramp time Δt . With the exception of the February 1998 data, the data points did not follow the Froissart-Stora prediction, which was shown in Figure II.3. We fit the July 1998 and October 1998 graphs data using the empirical equation:

$$P_f = P_i[(1 + \eta_M)e^{-\frac{(\pi \epsilon f_c)^2}{(\Delta f / \Delta t)}} - \eta_M], \quad (\text{IV.86})$$

where η_M is the maximum spin-flip efficiency, and ϵf_c is the normalized resonance strength. This equation is a modified Froissart-Stora formula, incorporating an imperfect maximum spin-flip efficiency parameter η_M ; recall that the Froissart-Stora formula (Equation I.7) predicts a 100% efficiency at very long ramp times.

To fit the October 1997 and February 1998 data, this empirical formula had to be even further modified. In these runs, a flat region was observed at very short ramp times of up to about 10 ms. To fit this flat region, we empirically raise the exponent in Equation IV.85 to the second power to yield:

$$P_f = P_i[(1 + \eta_M)e^{-\left(\frac{(\pi \epsilon f_c)^2}{(\Delta f / \Delta t)}\right)^2} - \eta_M]. \quad (\text{IV.87})$$

The fit parameters in both cases include: the initial beam polarization P_i , the maximum spin-flip efficiency η_M and the normalized resonance strength ϵf_c ; these parameters are listed in Table IV.3.

Note that for the October 1997, July 1998 and October 1998 data, the resonance strength, measured by spin-flipping, was much smaller than the mapped resonance width; in fact the spin-flipping resonance strength was quite close to the predicted

Run date	Oct. 97	Feb. 98	July 98	Oct. 98
P_i	0.738	0.721	0.582	0.691
η_M	0.720	0.750	0.940	0.815
ϵf_c (Hz)	513	283	500	286

Table IV.3: Fit parameters for spin-flipping by varying the ramp time at 104.1 MeV.

value of about 600 Hz. For the February 1998 data, both the mapped resonance width and the resonance strength measured by spin-flipping agree very well. This may be another indication that the apparent resonance width increase is due to some rf structure of the beam and not a manifestation of the rf depolarizing resonance's actual strength.

We also attempted to spin-flip a horizontally polarized beam using the vertical-field rf dipole described in Chapter III. The radial beam polarization after a single spin-flip is plotted against the rf dipole's ramp time in Figure IV.5. Note that the maximum beam polarization after spin-flip was only about 23%, while the initial polarization was 60%; this indicates a spin-flipping efficiency of only about 38%. Note also that, up to about 100 ms, the final polarization direction is not yet reversed; this suggests that the rf dipole-induced depolarizing resonance is very weak. Fitting the data using Equation IV.85, while ignoring the data point at 1000 ms, we get a normalized resonance strength ϵf_c of 240 Hz. As in the case of the rf solenoid-induced depolarizing resonance, this normalized strength is much smaller than the measured width w , and agrees better with the prediction given by Equation IV.84.

Probably, the low rf-dipole spin-flip efficiency is due to the rf dipole's weak field.

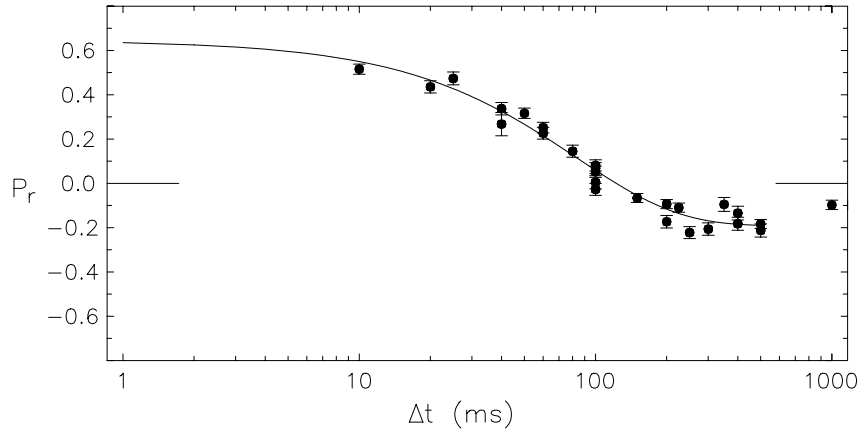


Figure IV.5: Spin-flipping while varying the rf dipole's ramp time. The measured radial beam polarization at 104.1 MeV is plotted against the ramp time Δt .

We plan to install a variable capacitor in parallel with the rf dipole to form an LC resonant circuit, similar to the rf solenoid's. This resonant circuit may help to increase the voltage across the rf dipole, and thus its magnetic field and resonance strength.

IV.4.3 Spin-flipping by varying the frequency range

After determining the optimum ramp time, we set Δt to that optimum value, which was, for example, 100 ms in October 1997, as indicated in Figure IV.4. We then studied spin-flipping while varying the frequency range to determine its optimal setting. Figure IV.6 shows the measured radial beam polarization plotted against the frequency range Δf at a fixed ramp time; the ramp time for each curve is shown on the graph.

Most of the Δf curves have a rather pronounced maximum where the spin-flipping efficiency is the highest. The very narrow maximum in the 15 ms data from February 1998 indicates that this 15 ms ramp time was too short; thus even a small increase in the resonance crossing rate $\Delta f/\Delta t$ due to a frequency range increase, significantly reduced the spin-flip efficiency; when the ramp time was increased to 50 ms, the maximum became much broader. For practical applications of spin-flipping in high-energy scattering experiments, it would be desirable to have some freedom in choosing the spin-flipper parameters; longer ramp times allow more freedom with the Δf choice. However, as was mentioned in Section VI.4, the spin-flipping efficiency seems to drop at very long ramp times.

Note that both the October 1997 and July 1998 data were taken with a ramp time Δt of 100 ms. However, in October 1997 the spin-flip polarization remained at a high value of about 60% for Δf of up to about 25 kHz, while in July 1998, it remained large only up to about 7 kHz and then decreased to zero near 15 kHz and then changed sign. Since the resonance crossing rate $\Delta f/\Delta t$ was the same for both data sets, the data may indicate that the actual resonance strength was probably much larger

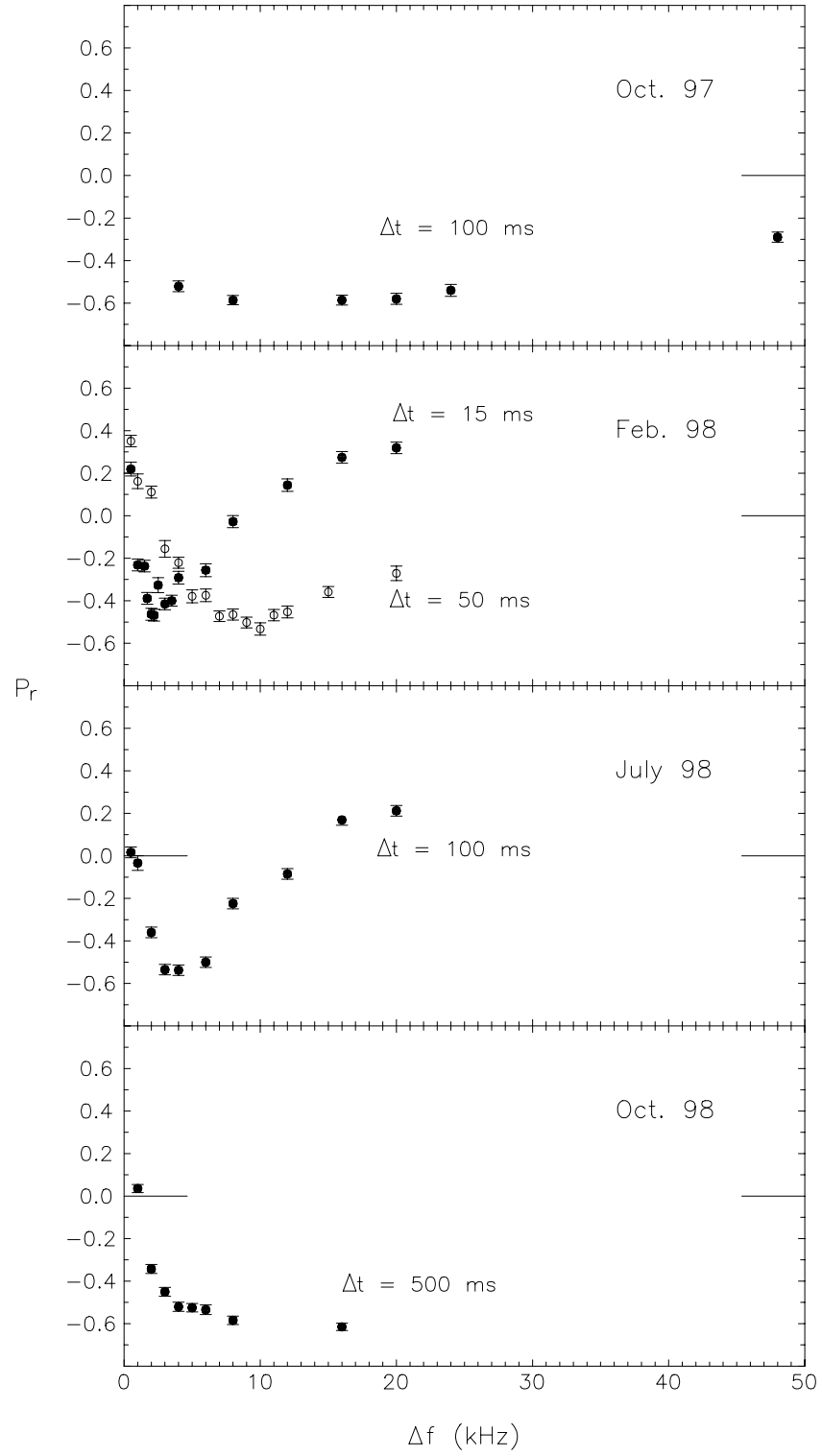


Figure IV.6: Spin-flipping by varying the rf solenoid's frequency range. The measured radial beam polarization at 104.1 MeV is plotted against the frequency range Δf .

in October 1997 than in July 1998; this allowed more efficient spin-flipping even at faster ramps. Another possible explanation is that the synchrotron sidebands were present around the main resonance in July 1998, which could reduce the spin-flipping efficiency.

In the October 1998 data, we saw the polarization decrease only at small values of Δf , while it was fairly flat in the frequency ramp range of 4 to 16 kHz; this was probably due to a very long ramp time of 500 ms. The resonance crossing rate $\Delta f/\Delta t$ was then sufficiently slow for a nearly complete spin-flip even at high Δf . Moreover, the polarization decrease at values of Δf below about 4 kHz resembles the shape of the rf depolarizing resonances, discussed in Section IV.2.

Recall that, in Figure IV.6, a frequency range of Δf represents varying the rf solenoid's frequency from $f_r - \Delta f/2$ to $f_r + \Delta f/2$. The HWHM (half-width at half-maximum) is the point on the curve where the polarization is 1/2 of the maximum polarization; this HWHM Δf width should be equal to the measured width of the resonance. Indeed, in the July 1998 and October 1998 curves, the HWHM Δf defined this way was about 2 kHz, which is very close to the measured widths of 2260 Hz and 1810 Hz, shown in Table VI.2. The February 1998 data with $\Delta t = 15$ ms has a HWHM in Δf of approximately 1 kHz, while the February 1998 data with $\Delta t = 50$ ms has a HWHM in Δf of about 4 kHz; both are very different from the 387 Hz, shown in Table VI.2. However, the polarization is positive at very low Δf . This may indicate that the resonance frequency f_r for Figure VI.6 may have shifted slightly by an amount δf_r from the measured position when it was mapped; the frequency ramp then may have started not exactly at $f_r - \Delta f/2$, but closer or further away from the resonance. For $\Delta f/2 = \delta f_r$, the frequency sweep would either start or end exactly on the resonance; thus one could then expect complete a depolarization of the beam. For $\Delta f/2 < \delta f_r$ the resonance would not be crossed, so there would only be partial depolarization without spin-flip.

IV.4.4 Multiple spin-flipping

With the ramp time and frequency range set to maximize the spin-flip efficiency, we performed multiple spin-flipping with the rf solenoid by crossing the resonance several times and measuring the beam's polarization after these multiple crossings. This technique was used to obtain a much more precise measurement of the spin-flip efficiency.

We did not perform multiple spin-flipping in the October 1997 run due to lack of beam time. However, the multiple spin-flip data for the February 1998, July 1998 and October 1998 runs are shown in Figure IV.7; in each graph, the radial beam polarization is plotted against the number of spin-flips. We always flipped the beam protons' spins an even number of times, so that the polarization direction after multiple spin-flipping was the same as the initial polarization direction. The magnitude of the final polarization was generally reduced by some depolarization during each spin-flip. We fit the multiple spin-flip data using

$$P_n = P_i \eta^n, \quad (\text{IV.88})$$

P_n is the beam's polarization after n spin-flips, P_i is the beam's initial polarization, and η is the efficiency of a single spin-flip. The maximum spin-flip efficiencies achieved in each experimental run are summarized in Table IV.4. Note that the efficiencies measured in multiple spin-flipping are significantly higher than those measured by a single spin-flip.

Run date	Oct. 97	Feb. 98	July 98	Oct. 98
η_M (single flip)	0.720 ± 0.025	0.750 ± 0.070	0.940 ± 0.050	0.815 ± 0.025
η (multiple flips)	-	0.910 ± 0.010	0.987 ± 0.004	0.950 ± 0.010

Table IV.4: Summary of spin-flipping efficiencies

Indeed, the observed polarization loss in the first spin-flip is generally higher than in the following flips. For example, in the February 1998 run, the polarization dropped by about 25% in the first spin-flip, while in each following spin-flip the loss was only about 9%. This higher polarization loss in the first spin-flip may be due

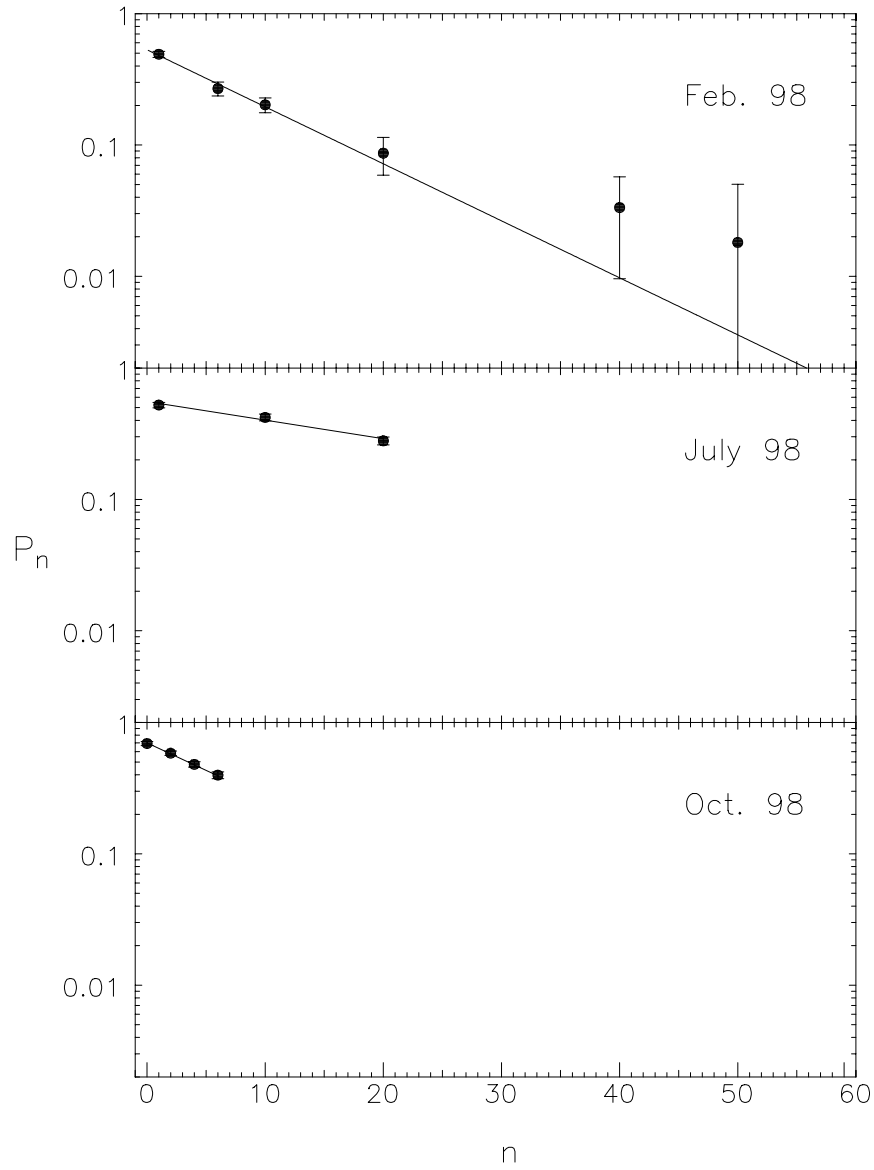


Figure IV.7: Multiple spin-flipping using the rf solenoid. The measured radial beam polarization at 104.1 MeV is plotted against the number of spin-flips n .

to improper alignment of the stable spin direction inside the rf solenoid with respect to the rf solenoid's longitudinal magnetic field. With a full longitudinal Siberian snake in the S section of the Cooler Ring, as was shown in Figure III.4, the stable spin direction (SSD) at 104.1 MeV was at an angle of approximately 60° to the rf solenoid's longitudinal field in the G section. The best spin-flipping results should occur when the SSD is perpendicular to the rf field direction. If the SSD makes an angle $90^\circ - \alpha$ with respect to the rf field, then the spin-polarization vector's rotation around the rf field could smear out the polarization, so that the polarization P_f after a single flip would be reduced by $\cos \alpha$. Since α is about 30° at 104.1 MeV, the beam polarization after one spin-flip would then be reduced by $\cos 30^\circ \simeq 0.87$ thus limiting the single spin-flip efficiency by this value. In further spin-flips this effect apparently does not play a role. Thus, total efficiency of the first spin-flip is a product of $\cos \alpha$ and the spin-flip efficiency measured using multiple flips.

For the February 1998 and October 1998 data, this hypothesis produces rather good agreement with the data, giving single spin-flip efficiencies of 0.79 and 0.82, respectively, using $\alpha = 30^\circ$ and the measured multiple spin-flip efficiencies. However, for the July 1998 data the calculated single spin-flip efficiency was about 0.85, while it was measured to be 0.943. It is likely that there are some subtleties in the spin-flipping process, which are not yet understood.

CHAPTER V

CONCLUSIONS

Our 1997-1998 experiments at the IUCF Cooler Ring show that it is possible to use a longitudinal rf magnet (rf solenoid) to spin-flip a horizontally polarized proton beam in the presence of a full Siberian snake. In July 1998, we reached a maximum spin-flipping efficiency of $98.7 \pm 1\%$ in multiple spin-flips by adjusting the rf solenoid's frequency ramp time and frequency range. This efficiency corresponds to about a 1.3% polarization loss per spin-flip; with an initial beam polarization of 70%, this leads to a polarization of about 36% after 50 flips.

However, due to the Lorentz contraction of an rf solenoid's longitudinal magnetic field integral, the strength of an rf-solenoid-induced depolarizing resonance decreases at higher beam energies, which makes an rf solenoid impractical for spin-flipping in high energy storage rings such as RHIC and HERA. An rf-dipole magnet, whose transverse $\int B \cdot dl$ is independent of the beam energy seems more suitable for efficient spin-flipping at high energy.

Studies of rf-dipole spin-flipping a vertically polarized stored proton beam at the IUCF Cooler Ring with no Siberian snake present were quite successful; a spin-flip efficiency of $96.7 \pm 1.0\%$ was achieved [43]. However, in the presence of a nearly full Siberian snake, spin-flipping a horizontally polarized proton beam with an rf-dipole has so far had little success; the maximum spin-flip efficiency was below 40%. The

main reason for this low spin-flip efficiency may be the weaker strength of our vertical rf dipole, whose $\int B dl$ was only about 2% of the rf solenoid's. We are currently working on increasing the rf-dipole spin-flipping efficiency for a horizontally polarized beam; we plan to try increasing the existing rf dipole's strength by using an LC resonant circuit, and way later build a new, higher-field rf dipole.

We also found that the measured widths of depolarizing resonances, created by both the rf solenoid and the rf dipole, were often much larger than the width predicted by the measured resonance strength, which was obtained from the spin-flipping data, and agrees quite well with theoretical predictions. We recently studied this relation between width and strength at the IUCF Cooler Ring [10]; a preliminary conclusion of these studies is that the apparent widening of the resonance may be due to the complex rf structure of the beam. Reducing the rf solenoid's or rf dipole's $\int B \cdot dl$ by a factor of 2 did not significantly reduce the measured resonance's width. However, turning off the rf acceleration cavities, which may generate this beam structure, reduced the measured resonance width by a factor of about 2.

APPENDIX

APPENDIX A**CE-69 COLLABORATION**

University of Michigan: V.A. Anferov¹, B.B. Blinov, M.A. Bychkov², E.D. Courant³, Ya.S. Derbenev, A.D. Krisch, W.B. Lorenzon, W.A. Peters, R.A. Phelps⁴, L.G. Ratner^{3†}, K.V. Sourkont², V.K. Wong

Indiana University Cyclotron Facility: C.M. Chu, S.Y. Lee, T. Rinckel, P. Schwandt, B. von Przewoski

HEARO (INS and KEK), Japan: C. Ohmori, H. Sato, T. Toyama

Fermilab: P.S. Martin, A.D. Russell

King Fahd University: F.Z. Khiari

SLAC: A.W. Chao, M.G. Minty

¹ now at IUCF

² also at Moscow State University

³ also at Brookhaven National Laboratory

⁴ now at IBM, Inc.

† deceased

Note: The institutions listed are the institutions where each person was primarily working during the CE-69 experiment (1997-1998). Many people have since moved.

BIBLIOGRAPHY

BIBLIOGRAPHY

- [1] T. Khoe *et al.*, Part. Accel. **6**, 213 (1975).
- [2] F. Z. Khiari *et al.*, Phys. Rev. D **39**, 45 (1989).
- [3] J. L. Laclare *et al.*, Jour. de Phys. **46**, C2-499 (1985).
- [4] H. Sato *et al.*, Nucl. Instrum. Methods A **272**, 617 (1988).
- [5] Ya. S. Derbenev and A. M. Kondratenko, Part Accel. **8**, 115 (1978).
- [6] M. Froissart and R. Stora, Nucl. Instrum. Methods **7**, 297 (1960).
- [7] L. H. Thomas, Philos. Mag. **3**, 1 (1927).
- [8] V. Bargmann, L. Michel and V. L. Telegdi, Phys. Rev. Lett. **2**, 435 (1959).
- [9] D. A. Crandell, Ph.D. dissertation, University of Michigan (1996).
- [10] V. A. Anferov *et al.*, Phys. Rev. ST Accel. Beams **3**, 041001 (2000).
- [11] A. D. Krisch *et al.*, Phys. Rev. Lett. **63**, 1137 (1989).
- [12] J. E. Goodwin *et al.*, Phys. Rev. Lett. **64**, 2779 (1990).
- [13] M. G. Minty *et al.*, Phys. Rev. **D44**, R1361 (1991).
- [14] V. A. Anferov *et al.*, Phys. Rev. **A46**, R7383 (1992).
- [15] R. Baiod *et al.*, Phys. Rev. Lett. **70**, 2557 (1993).
- [16] R. A. Phelps *et al.*, Phys. Rev. Lett. **72**, 1479 (1994).
- [17] B. B. Blinov *et al.*, Phys. Rev. Lett. **73**, 1621 (1994).
- [18] D. D. Caussyn *et al.*, Phys. Rev. Lett. **73**, 2857 (1994).
- [19] C. Ohmori *et al.*, Phys. Rev. Lett. **75**, 1931 (1995).
- [20] L. V. Alexeeva *et al.*, Phys. Rev. Lett. **76**, 2714 (1996).
- [21] D. A. Crandell *et al.*, Phys. Rev. Lett. **77**, 1763 (1996).
- [22] R. A. Phelps *et al.*, Phys. Rev. Lett. **78**, 2772 (1997).
- [23] B. B. Blinov *et al.*, Phys. Rev. Lett. **81**, 2906 (1998).

- [24] C. M. Chu *et al.*, Phys. Rev. **E58**, 4973 (1998).
- [25] B. B. Blinov *et al.*, Phys. Rev. ST Accel. Beams **2**, 064001 (1999).
- [26] J. E. Goodwin, Ph.D. dissertation, Indiana University (1990).
- [27] M. G. Minty, Ph.D. dissertation, Indiana University (1991).
- [28] B. S. van Guilder, Ph.D. dissertation, University of Michigan (1993).
- [29] C. M. Chu, Ph.D. dissertation, University of Michigan (1994).
- [30] V. P. Derenchuk and M. K. Wedekind, IUCF Scientific and Technical Report, 165 (1994).
- [31] G. I. Budker, Proc. of International Symposium on Electron and Positron Storage Rings, Saclay (1966); T. J. P. Ellison, Ph.D. dissertation, Indiana University (1990).
- [32] E. J. Stephenson, private communication.
- [33] S. W. Wissnik *et al.*, Proc. of the 7th International Conference on Polarization Phenomena in Nuclear Physics, Paris (1990).
- [34] B. von Przewoski *et al.*, Proc. of the 9th International Symposium on High Energy Spin Physics, Bonn, 607(1990).
- [35] G. Walters *et al.* Nucl. Instrum. Methods **153**, 401 (1978).
- [36] R. D. Ransome *et al.* Nucl. Instrum. Methods **201**, 315 (1982).
- [37] E. Aprile-Giboni *et al.* Nucl. Instrum. Methods **215**, 147 (1983).
- [38] M. W. McNaughton *et al.*, Nucl. Instrum. Methods **A241** 435 (1985).
- [39] A. D. Krisch *et al.* Snake Depolarizing Resonances and Full Snake Spin-Flipping. Proposal submitted to IUCF PAC (1997); approved as IUCF experiment CE-69.
- [40] G. Dome, Theory of RF Acceleration, CERN Accelerator School, Advanced Accelerator Physics Course **1** 110 (1985).
- [41] R.A. Phelps, presentation at CE-40 meeting, 28 June 1994.
- [42] M. Bai *et al.*, Phys. Rev. Lett. **80**, 4673 (1998).
- [43] B.B. Blinov *et al.*, Bull. Am. Physical Soc. **45**, No. **2** (2000) 85.